OAK RIDGE NATIONAL LABORATORY
MANAGED BY UT-BATTELLE FOR THE DEPARTMENT OF ENERGY

ORNL/TM-2011/ 338

ORNL ADV Post-Processing Guide and MATLAB Algorithms for MHK Site Flow and Turbulence Analysis

September 2011

Prepared by

Budi Gunawan, Ph.D.
Vincent S. Neary, Ph.D., P.E.
James R. McNutt

UT-BATTELLE

ORNL/TM-2011/338

Environmental Science Division

ORNL ADV POST-PROCESSING GUIDE AND MATLAB ALGORITHMS FOR MHK SITE FLOW AND TURBULENCE ANALYSIS

Budi Gunawan, Ph.D.
Vincent S. Neary, Ph.D., P.E.
James R. McNutt

Date Published: September 30, 2011

Prepared by
OAK RIDGE NATIONAL LABORATORY
Oak Ridge, Tennessee 37831-6283
managed by
UT-BATTELLE, LLC
for the
U.S. DEPARTMENT OF ENERGY
under contract DE-AC05-00OR22725

CONTENTS

LIST OF FIGURES

LIST OF TABLES

NOTATION

$C1$	first reconstruction constant, a calibration parameter in mPST	(-)
$C2$	second reconstruction constant, a calibration parameter in mPST	(-)
f	frequency band	(-)
f_R	sampling frequency	(Hz)
H	flow depth in the main channel	(m)
L_x	energy containing length scale/macroscale turbulence	(m)
$nwin$	number of window	(-)
RMS	root mean square or standard deviation, $\sqrt{\frac{\Sigma {x_i}^2}{n}}$	(the unit of x)
u	instantaneous velocity in the streamwise direction	(ms^{-1})
u'	instantaneous velocity fluctuation in the streamwise direction	(ms^{-1})
U_c	convective velocity	(ms^{-1})
U	mean streamwise velocity with respect to time	(ms^{-1})
U_{RMS}	RMS value of the streamwise velocity	(ms^{-1})
v	instantaneous velocity in the lateral direction	(ms^{-1})
v'	instantaneous velocity fluctuation in the lateral direction	(ms^{-1})
V	mean lateral velocity with respect to time	(ms^{-1})
V_{RMS}	RMS value or standard deviation of the lateral velocity	(ms^{-1})
w	instantaneous velocity in the vertical direction	(ms^{-1})
w'	instantaneous velocity fluctuation in the vertical direction	(ms^{-1})
W	average vertical velocity with respect to time	(ms^{-1})
W_{RMS}	RMS value or standard deviation of the vertical velocity	(ms^{-1})
z	vertical distance from bed	(m)

ACKNOWLEDGMENTS

The authors thank DOE/EERE for supporting the development of the ORNL post-processing algorithms under CPS Project No. 20689, CPS Agreement Nos. 20065 and 20070. The pst_outlier, pst, mpst_outlier and mpst algorithms as they appear in the appendix originated from algorithms developed by Nobuhito Mori, of Tokyo University in Japan, who maintains a GNU license to the algorithms. The authors also thank Dr. Leonardo Chamorro and Mr. Craig Hill from the St. Anthony Falls Laboratory (SAFL), Minneapolis, Minnesota, for providing the original algorithm for plotting Power Spectral Density and acoustic Doppler velocimetry data from the SAFL , main channel.. Student interns who assisted with MATLAB code development and testing include Bennett Flanders, Pablo Rosado, Danny Sale, Andrew Hansen and Sreekanth Bangaru.

1 INTRODUCTION

Measurements of mean velocity, Reynolds stresses and turbulence spectra are desirable for marine and hydrokinetic (MHK) device testing, site development and environmental monitoring. The acoustic Doppler velocimeter (ADV) is the most practical and economical instrument for obtaining these measurements. Typical profiles, illustrated in Figure 1.1, allow assessment of the hydrodynamic forces acting on the hydrokinetic device and the power density and power available over the energy extraction plane (EEP). This data informs the MHK device and component design and estimation of performance curves, annual energy production (AEP) and cost of energy (COE).

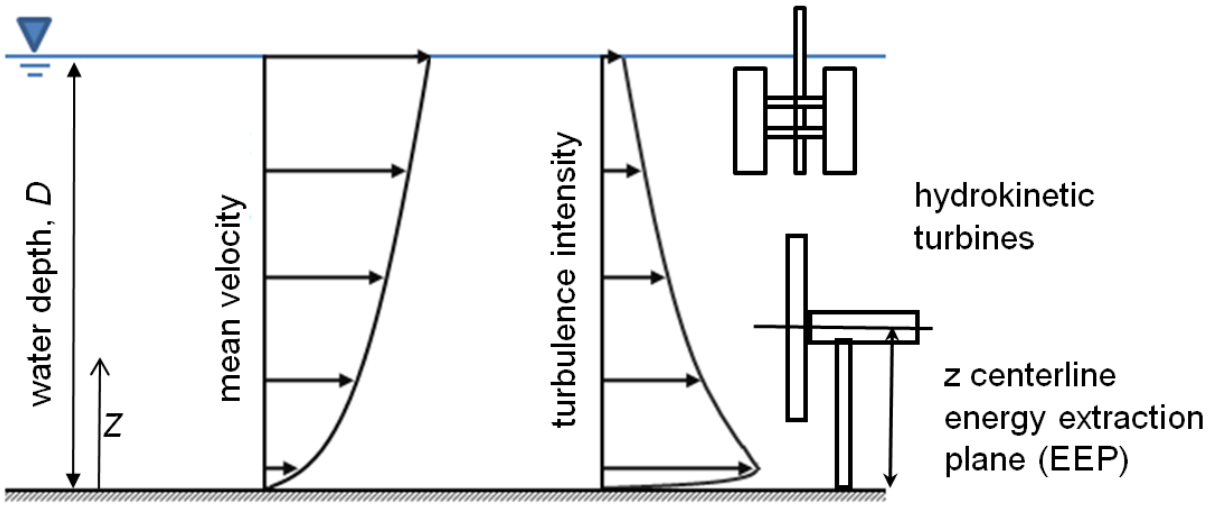

Figure 1.1 Typical distributions of velocity and turbulence and sketch of horizontal-axis hydrokinetic turbine. Modified from Neary and Sale (2010).

ADV measurements of mean velocity and turbulence are difficult in large rivers and tidal channels where depths commonly exceed several meters, currents are greater than 1m/s and surface waves and turbulence are generated by recreational boat and barge traffic in navigation channels. These conditions cause instrument displacement, motions and vibrations that can compromise measurement accuracy. These problems are exacerbated when deploying ADVs at large depths from tethered cables or stationary mounts and would be especially challenging if attempting measurements in the wake flow field downstream of the device. Given these challenges, there is a need to test and validate turbulent flow field measurement protocols, instrument packages, deployment strategies, and turbulence post-processing algorithms.

To the authors' knowledge there are currently no standard protocols for post-processing ADV measurements to ensure accuracy of velocity and turbulence data. There are also no standard post-processing algorithms that are consistently used for laboratory and field measurements. This report attempts to address this deficiency. Standard methods along with guidance for post-processing ADV measurements using MATLAB algorithms that were evaluated and tested by Oak Ridge National Laboratory (ORNL) are presented following an overview of the ADV

operating principles, deployment methods, error sources and recommended protocols for removing and replacing spurious data.

2 ACOUSTIC DOPPLER VELOCIMETRY

The ADV is a point-velocity measurement device that has been tested for a wide range of water current environments to measure one or more components of instantaneous velocity time series from which mean velocity, turbulence statistics and turbulence spectra are calculated. It was developed in 1992 for the U.S. Army Corps of Engineers Waterways Experiment Station to measure three dimensional flows in physical models with sub-centimeter resolution, a minimum of 25Hz sampling rate and a commercial unit cost of less than $10,000 (Lohrmann *et al*. 1994). The ADV is now a standard instrument for measuring velocity and turbulent statistics in the laboratory and the field.

ADVs are well suited to characterize the mean velocity and turbulence characteristics at discrete points (Thomson *et al*. 2010; Fox and Belcher 2009; Nikora and Goring 2004). Recent examples of acoustic measurements include those in flumes (Voulgaris and Trowbridge 1998), tidal channels (Thomson *et al*. 2010) and rivers (Holmes and Garcia 2008; Babaeyan-Koopaei *et al*. 2002). Measurements obtained using an ADV may contain errors that are mainly caused by Doppler noise and signal aliasing. The Doppler noise are affected by the instrument model, fluid characteristics and flow conditions that include flow velocity, presence and characteristics of suspended particles in the flow, and turbulence. The signal aliasing is due to the methodology used to calculate the velocity by the instrument (Nikora and Goring 1998; Cea *et al*. 2007). These errors can significantly increase the variance of the data, bias the mean velocity and alter the turbulence spectra, especially in the high frequency range.

A post-processing methodology capable of detecting errors is therefore crucial for assuring the quality of ADV data. These errors may appear as spikes in the data, or may appear as normal fluctuations in the velocity that are difficult to detect. If one is only interested in the measurement of the mean velocity, calculating the data after the spikes are detected and removed is generally sufficient. If one is interested in calculating the turbulence spectra, data replacement is necessary. It should be emphasized that data replacement is not aimed at reconstructing the dataset, which would have been measured when errors in the dataset do not exist, but rather to fill in data gaps to ensure that they are continuous with respect to time, which is the prerequisite for power spectra computations. The statistical properties of the dataset should be the same if not similar to the dataset after the errors are removed.

2.1 ADV PRINCIPLE OF OPERATION

The ADV probe includes one transmit transducer and three or four receive transducers (Figure 2.1**)**. An ADV can measure 2D or 3D water velocity components within a small sampling volume (of the order of $1cm^3$) at a short distance (typically 5 to 18cm) from the transmit transducer (Nortek 2009; SonTek 2011a; SonTek 2011b). As reported by the manufacturers, the ADV models that are designed for field measurements are capable of measuring velocities typically up to 5m/s within 1% accuracy and up to a 25Hz sampling rate. More advanced models can measure velocities up to 7m/s with sampling rates as high as 200Hz.

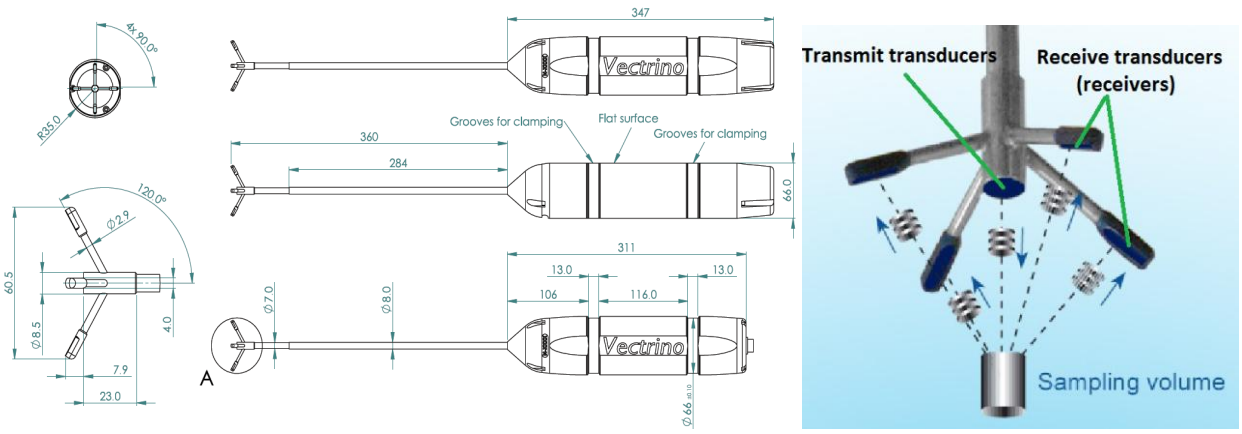

Figure 2.1 Illustrations of Nortek Vectrino ADV probe head with four receive beams (adapted from Nortek 2009).

An ADV operates by transmitting an acoustic pulse with a defined frequency and pulse duration. Three or four receive transducers (receivers) are positioned and focused on a finite (sampling) volume of space intersecting the transmitted beam path as shown in Figure 2.1. The transmitted acoustic pulse is reflected by suspended particles in water (or bubbles) to all directions. Only the echoes that are perpendicular to the receivers are recorded by the ADV. The recorded echo is shifted in frequency if the particles are moving towards or away from the receivers (radial motion with respect to the receivers). Angular motion of the particles with respect to the transducers causes a Doppler shift. This Doppler shifted frequency, measured by each receiver, is proportional to the component of the flow velocity along the receive beams. A minimum of three velocity components along the receive beams are required to reconstruct a 3D water velocity. A fourth receive transducer, which is available for some models, verifies the velocity data obtained.

Since the probe measures the velocity of the scattering particle and not the fluid itself, the operation of the system assumes that the scattering particles follow the fluid flow. The density of the particle relative to the fluid density and the particle size will influence the particle's ability to follow the fluid flow. Raffel *et al*. (2007) provide a discussion on tracer particle sizing. The particle relaxation time is a convenient measure of the tendency of a particle to attain equilibrium with the local fluid velocity. Scattering sources that do not follow the local flow will bias the measurement statistics.

Underwood (1994) provides a detailed discussion of the features, capabilities and operation of the ADV. The ADV sensor sampling volume, formed at the intersection of the transmitter and receiver beams, is typically a cylindrical volume on the order of several mm in diameter with a length that is comparable to the diameter. The sampling volume is displaced from the probe head due to the probe head design. The absolute displacement is a function of probe design and can vary from several cm to over 15cm.

More recent ADV models use a pulse-coherent method to calculate the Doppler shift. Instead of using only a single acoustic pulse, a pulse-coherent ADV uses a pair of coded acoustic pulses with a known time lag to measure the phase shift of the acoustic pulses (Figure 2.2). The phase-

shift is then converted to velocity by scaling to the speed of sound in water. Measuring phase-shift provides a more accurate result than direct determination of the Doppler Shift (Rusello 2009; RDI 1996). However, this method also introduces an ambiguity velocity, which is discussed in section 2.3.2. Further detailed explanation on the ADV principles can be found in references such as Rusello (2009) and Lohrmann *et al.* (1995).

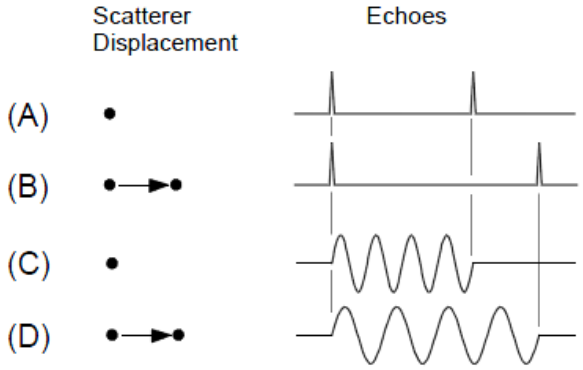

Figure 2.2 Time dilation and Doppler frequency shift. (A) and (B) compare echoes of pulse pairs from stationary and moving particles. (C) and (D) show the same for the echo from a sinusoidal pulse with a duration equal to the time between the two short pulses in (A) and (B). The vertical lines indicate that the stretching is the same for the two pulses as it is for the sinusoid (RDI 1996).

2.2 ADV DEPLOYMENT METHODS

Common ADV deployment methods include stationary deployments like those shown in Figure 2.3 and cable deployments such as an ADV deployed from a USGS sounding weight. Stationary measurements from a stable platform are required for long term measurements on the order of weeks to months. For profiling with short sampling durations on the order of ten minutes, cable deployments like that shown in have been successfully used (Holmes and Garcia 2008**).** For the cable deployment shown in Figure 2.4 the cantilevered arm is kept short to minimize arm vibration but must be long enough to position the sample volume out of any weight induced flow variations. Cable deployed ADVs may allow a greater number of measurement points compared to stationary mounted ADVs. However, it is difficult to accurately position the sampling volume at the desired locations in the water column. In addition, the spatial stability or stable position holding capacity of the sounding weight may be compromised in the wake of an MHK device or underwater obstruction. The sounding weight may exhibit oscillatory motion or vibration in response to the intermittent, rotating blade wakes downstream of an MHK device. This flow induced motion will be transferred to the ADV probe upstream of the weight resulting in increased uncertainty in the 3-component ADV measurement due to sample volume motion and varying probe alignment relative to the true flow direction. For deep water deployment, autonomous underwater vehicles (AUV) and remotely operated vehicle (ROV) as shown in Figure 2.5 can be used (e.g., Zhang *et al.* 2001).

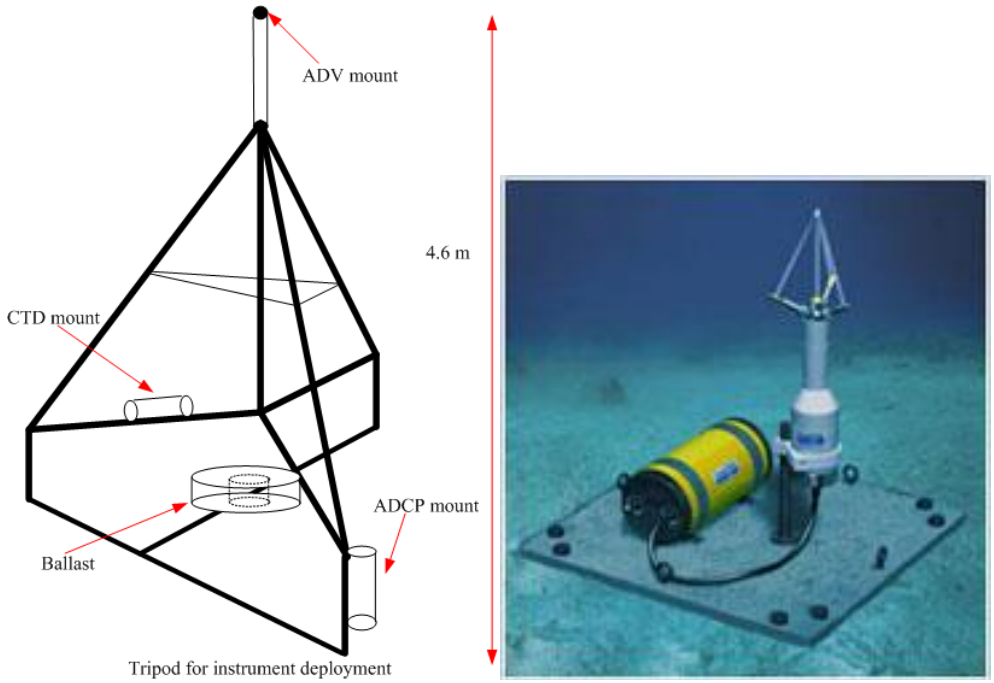

Figure 2.3 Left: Stationary tripod deployed ADV used for Marrowstone Island, WA deployment (Richmond *et al.* 2010); Right: Bed mounted ADV deployment (SonTek 2011).

Figure 2.4 Cable deployed Nortek Vectrino ADV with sounding weight (Photo courtesy of Robert Holmes, USGS).

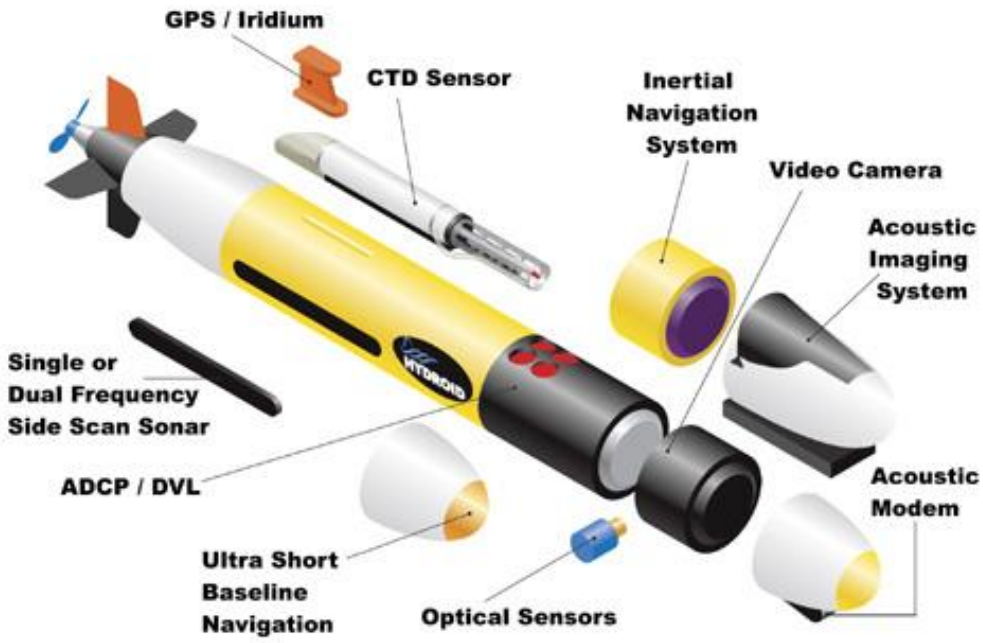

Figure 2.5 Remus 600 AUV (Hydroid, Inc. 2011).

2.3 ADV ERROR AND SIGNAL PROCESSING METHODS

Many investigators have addressed sources of error and the impact of noise on turbulence measurements (Hurther and Lemmin 2001; Finelli *et al*. 1999; Voulgaris and Trowbridge 1998; Nikora and Goring 1998). Spatial resolution filtering, the signal acquisition/ sampling frequency selected, signal processing and system noise can compromise measurement accuracy. Sample rate and signal processing can cause a low-pass temporal filtering as well as a velocity alias error. System noise, which typically includes sampling errors (channel drop-outs or loss of coincidence), Doppler noise, gradient errors and multi-probe signal contamination can also bias mean and turbulence velocity estimates. Some of these noise sources can be scale or frequency dependent. Apart from these systematic errors, human error such as inaccuracy in aligning the ADV probe (Ansar and Nakato 2001) can alter the data significantly. Sections 2.3.1 – 2.3.5 describe the type of errors that may be encountered when using an ADV.

2.3.1 Boundary interference

ADVs measure the acoustic Doppler shift, so unexpected reflections of the transmitted signals have the potential to severely compromise the integrity of collected data. Unexpected reflections may occur if an acoustic pulse that has encountered a boundary is received during the same interval as data reflected from the particles within the sampling volume causing a velocity hole (Lane *et al.* 1998) or weak spot (Craig *et al.* 2010). The effects of boundary interference are most pronounced and of significant concern when the boundary enters into the sampling volume. Finelli *et al.* (1999) explored the effects of sample volume proximity to the boundary on measurements acquired by ADV instruments. Having empirically measured the size of the sampling volume, they found it to be substantially larger than the nominal value provided by the

manufacturer. In their literature, they include their method for measuring the sample volume and caution users of the importance of appropriately positioning the device in order to extract meaningful data.

2.3.2 Signal aliasing

Prior to deployment and data collection the ADV user must specify the range of velocities that is expected to be sampled in the flow. Aliasing or over-ranging causes an ambiguity velocity that arises from particles in the sampling volume moving toward the transducers at a rate beyond that prescribed by the user. Phase shift can only be measured in the range 0^o – 360^o. Hence, the measurement will start again from 0^o once phase passes 360^o. In such a case, an abrupt change in the velocity (a spike) is likely to occur with a change in sign (Figure 2.6). For open channel flows this will bias the mean streamwise velocity towards lower value.

While some ADVs allow for velocity ranges approaching a magnitude of five meters per second, which would encompass any smaller ranges and practically eliminate the problem of over-ranging, the greater the velocity range setting results in an increased production of noise by the instrument. The effects of noise can also seriously affect the accuracy of data, and so the selection of the velocity range should be carefully considered. It is important for the user to assess the anticipated range of unsteady velocities that may be encountered in any flow component.

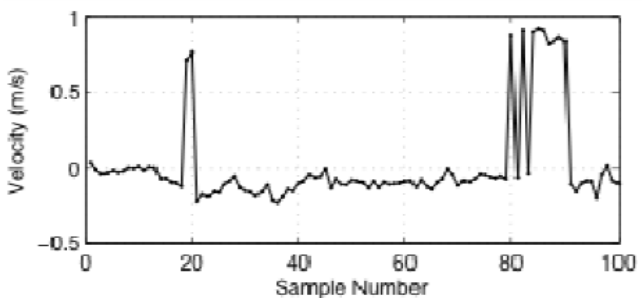

Figure 2.6 An example of phase wrapping recorded with an ADV with 50Hz sampling frequency (Rusello 2009).

2.3.3 Doppler noise

Often spurious data do not manifest as spikes but as underlying noise. This is especially relevant in the case of ADV technology since the devices themselves produce a Doppler noise, appears in the data as white noise, which affects high statistical moments and obscures trends in the power spectra. The magnitude of Doppler noise is affected by instrument model, fluid characteristics and flow conditions that include flow velocity, presence and type of particles in the flow, and turbulence (Nikora and Goring 1998). Nikora and Goring (1998) attempted to quantify the Doppler noise by measuring velocity of still water with different seeding particles and ADV velocity range settings. They showed that the magnitude of the Doppler noise for different spectra bands is more or less the same. They then used the result to correct velocity measurements with the same ADV velocity range setting. Figure 2.7 shows the typical auto-spectra plot for the longitudinal velocity component and the white noise level measured in an

outdoor flume. Doppler noise in still water appears as white noise. However, correcting the auto-spectra of moving water velocity with the white noise obtained from still water measurement is not appropriate when the magnitude of the Doppler noise is changing with increased water velocity. Note that the velocity spectra begin to flatten at higher frequencies at the same order of magnitude with the average Doppler noise. Voulgaris and Trowbridge (1998) introduced the term 'noise floor' to describe the flat power spectra density, which also correspond to the total noise of the instrument. The noise floor may not be apparent unless sampling at sufficiently high sampling rates.

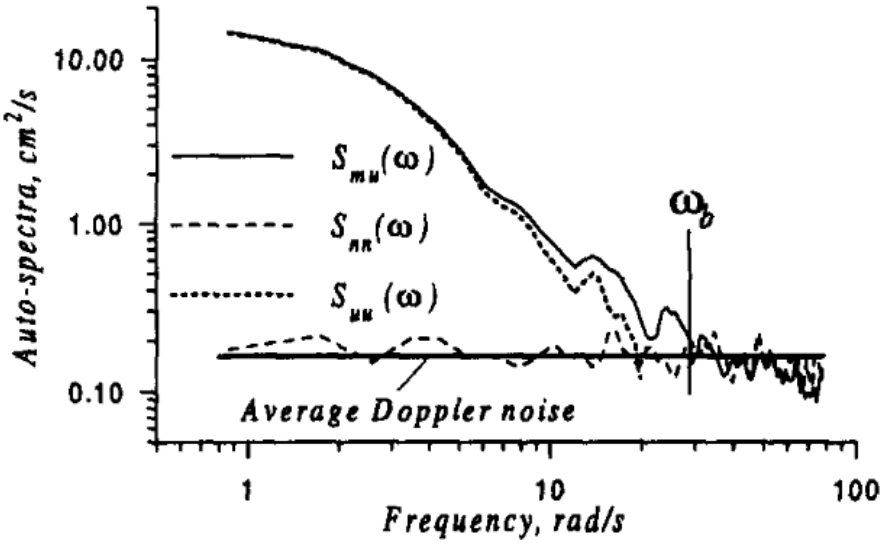

Figure 2.7 Typical auto-spectra for longitudinal velocity component and white noise level calculated from measured Doppler Noise (Nikora and Goring 1998).

2.3.4 Spatial averaging

Although an ADV measurement is considered a 'point' measurement, it is in fact an average over a sample volume with spatially non-uniform velocities. As a result errors associated with spatial averaging are present. Again, the user should be cognizant of the flow scales of interest when selecting a measurement device. A large measurement volume will spatially low-pass filter the velocity field and may bias the statistics away from small scale structures that may be important for unsteady loading and system vibration and noise.

2.3.5 Temporal averaging

The frequency at which ADVs measure the instantaneous velocity is greater than the sampling frequency of the data provided to the user. The ADV data ultimately collected at the sampling frequency are in fact averages calculated internally. The averaging process is a digital non-recursive filter (Hamming 1983; Bendat and Piersol 1971). This filtering affects the power spectrum by removing energy bands beyond the cut-off frequency and reduces the even moments of the signal (García *et al*. 2005). The frequency limit in the measured data will typically be at least ½ the sampling frequency due to the Nyquist criteria and may be even lower due to processing constraints.

2.4 PROTOCOLS FOR REDUCING ERROR

The majority of common errors may be avoided with the application of a few simple protocols outlined below.

2.4.1 ADV calibration file and beam check

Every ADV has a unique calibration file created after factory calibration. The user should check that the ADV serial number matches that of the calibration file and upload this file to the instrument before measurements. If this is not done, or the wrong calibration file is loaded, the user should be notified. If this notification is ignored the measurements will be invalid. A beam check should be performed before and after measurements as detailed by SonTek (2001). An example screen shot using the Horizon ADV software (SonTek 2007) is shown in Figure 2.8. The peak position and levels of all beams should be the same within some specified tolerance.

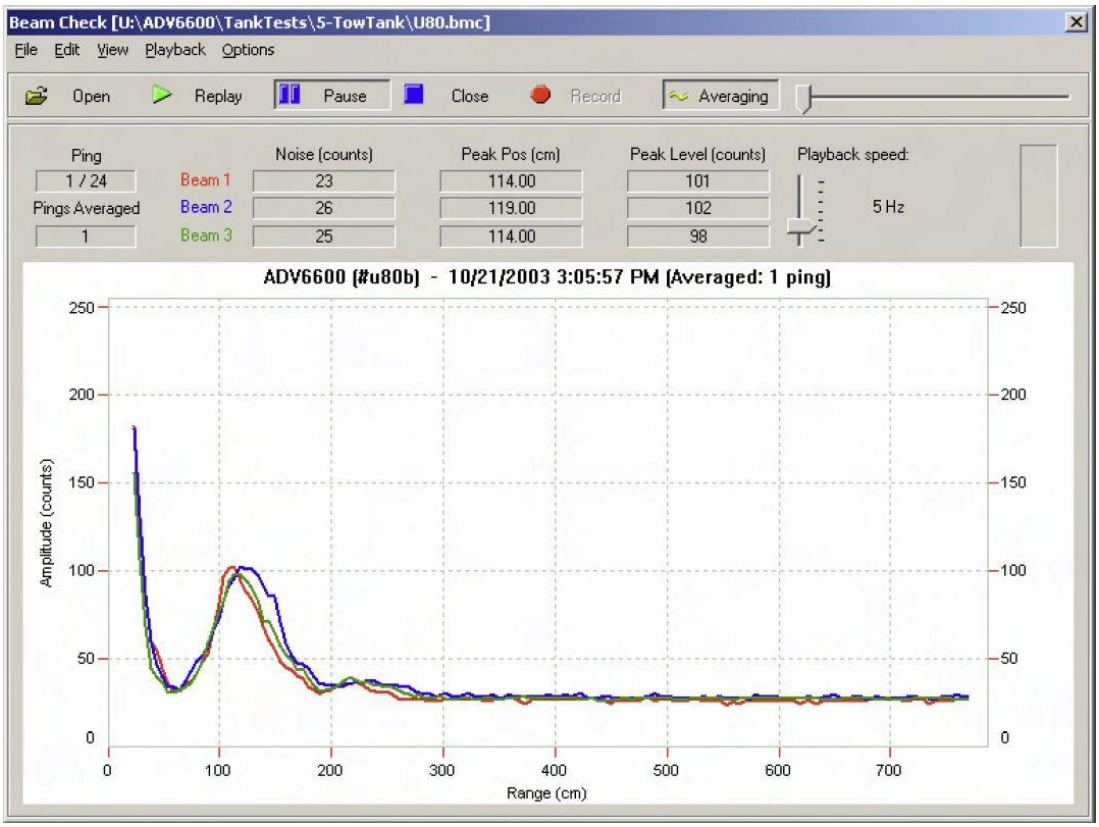

Figure 2.8 Example beam check using Horizon ADV software (SonTek 2007).

2.4.2 Determining the vertical size of the sample volume

The identification of the boundaries of the sampling volume is important so that the validity of the data is not being compromised by boundary interference that may occur when the ADV is in close proximity to solid boundaries (e.g., moorings, cables). Specifications on the dimensions and placement of the sample volume provided by manufacturers are imperfect. Therefore, in order to enhance the reliability of data sampled by these devices it is important to determine the actual size of the sampling volume with greater certainty. Finelli *et al.* (1999) describes the

method which they implemented for measuring the dimensions of the sampling volumes of their devices. They created an acoustic target using two lengths of monofilament fishing line stretched across the interior of a water tank such that the lines intersected at near right angles in the center of the tank. The water was allowed to sit for a substantial length of time so that any suspended gases could be released and any sediment could settle. The probe was positioned directly over the target at a sufficient distance so that the sampling volume did not encompass the target, i.e., the SNR was uninfluenced by the target and data were sampled for ten seconds. The instrument was then lowered slightly and another set of data were sampled. This process was continued until the sampling volume had passed the target entirely. Calculating the average SNR for every sample, the researchers were able to identify the bounds at which the target began to influence the data and so identify the bounds of the sampling volume.

2.4.3 Dimensionless frequency criteria

García *et al.* (2005) defined a dimensionless frequency for analyzing whether an instrument is capable of providing a good description of turbulence. They presented the following inequality:

$$F = \frac{f_R L}{U_c} > 20 \tag{2.1}$$

where F, f_R , L, and U_c are the dimensionless frequency, sampling frequency, energy containing length scale, and convective velocity respectively. They concluded that F should be greater than 20 to obtain a good description of the flow turbulence using ADVs and ensure that important portion of the velocity spectrum is resolved.

2.4.4 Histogram inspection

Effects of over-ranging on data are easy to identify. The probability density function (PDF) of a time series (in the beam coordinate system) may demonstrate a sudden velocity cut-off beyond which no data will be registered. If this abrupt discontinuity is observed in a data sample, the user should increase the user defined velocity range until the histogram of the time series no longer demonstrate such characteristics. Optimally the user should select the smallest velocity range (in either beam or earth coordinates) for which no cut-off is observed in the histogram.

2.4.5 Methods for error reduction

In cases where spurious data cannot be avoided, the data can be reconstructed so that the assumptions drawn from the data are representative of the characteristics of the flow. Several methods that are often used are described.

2.4.5.1 Data filtering based on correlation coefficient values

Correlation is a measure of the similarity of two pulse echoes being measured by the Doppler instrument. Zero correlation means the two echoes are unrelated, where as a correlation of 1 means the two echoes are identical. High correlation is desired because it indicates confidence that the system measured the two pulses it originally sent out and is determining a valid phase shift. In practice correlations of zero are not observed because of noise due to electronics,

temperature fluctuations, and other factors. Correlation reported by the instrument will be on a percent scale from 0-100%, so simply multiplying the limits, zero to one, by 100 will place them in the appropriate range. Many users use correlation thresholds around 70% for screening bad data, but a generalization to some universal value is unwarranted. A close examination of the dataset is in fact the best way to set a correlation threshold (if any) for discarding bad data points.

2.4.5.2 Spike Identification, removal and replacement

Baldwin *et al.* (1993) and Petrie *et al.* (1988) first applied a velocity hodograph elliptical filtering technique to laser Doppler velocimeter (LDV) measurements as an effective means of filtering LDV measured noise. In this technique, the measured data are rotated into the principal stress coordinates and an elliptic filter of size *N* principal stresses in the minor and major axes is applied to the 2D probability density function (PDF). Velocity ensembles occurring outside the defined ellipse are filtered from the data set. Fontaine *et al.* (1996) extended the 2D elliptic filter technique to the 3D flow application with a principal stress 3D ellipsoid filter on three-component LDV measured data.

The Phase-Space Thresholding (PST) technique, developed by Goring and Nikora (2002), is another ellipsoidal filter technique where invalid points are identified as those lying outside of the universal threshold defined ellipsoid in a 3D Poincaré phase space. While the ellipsoidal filter technique of Fontaine *et al.* (1996) operates on the instantaneous velocity hodograph (*u* vs *v* vs *w*) with filtering applied in the principal stress space, the PST technique operates on the instantaneous velocity and it's local accelerations (*u* vs *du/dt*). The PST technique has been critically analyzed and improved upon by a number of peers (Parsheh *et al.* 2010; Wahl 2003).

The use of the PST algorithm has grown in acceptance and is now the standard means of filtering data. Nevertheless, improvements to the PST algorithm have been proposed to address the main criticism that it was replacing valid data around spikes. While removal has negligible effects on the value of bulk statistical moments, it has been shown by (Parsheh *et al.* 2010) to compromise time-dependent indicators such as the power and energy spectra. Goring and Nikora (2002) have suggested cubic interpolation by the twelve points on either side of an identified invalid datum and they seem to be one of the few researchers to have compared various methods. Parsheh *et al.* (2010) have proposed a modified Phase-Space-Thresholding Sample and Hold algorithm (mPST-SH) that evaluates the validity of data in three stages: first, any velocity measurements near the average are incontrovertibly marked as valid; then, any data far from the average are marked as invalid and are removed; and finally, the data are filtered using the PST technique.

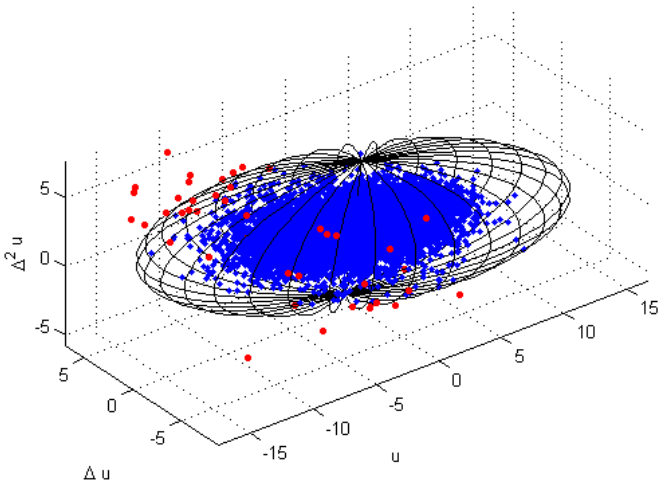

Figure 2.9 An example of Phase-Space threshold filtered plot.

2.4.5.3 Data processing in beam coordinates

Data is always measured in beam coordinates, but ADV software generally allows the user to select the coordinate system for data output, including beam, Cartesian (*XYZ*) or Earth East North Up (*ENU*) coordinates. As previously discussed, over-ranging occurs when particles in the sampling volume move toward one of the transducers at a rate beyond that prescribed by the user. When analyzing the measured Doppler phase shift, such data cannot always be resolved and the associated velocity is erroneously translated into the assigned velocity range resulting in a spike in the data. It is recommended that all acoustic measurements should be recorded and processed in beam coordinates because the spike only occurs in one of the beam coordinate time series. If coordinate transformation is employed before such a spike is removed, the spike may be obfuscated by the linear transformation and also may affect the other components, rendering identification of the spike more difficult. Therefore, it is suggested that users always record data in the beam coordinate system and only after appropriate error removal procedures have been implemented converted to another coordinate system (e.g., Doroudian *et al*. 2007).

2.4.5.4 Spectral noise filter

A spectral analysis technique by Voulgaris and Trowbridge (1998) was suggested by Goring and Nikora (1998) for removing the effects of noise within the noise floor of the power spectra at higher frequencies by the average of the noise spectrum. The empirical spectra of the Doppler noise are replaced by straight horizontal lines whose ordinates are equal to the average of the noise spectral ordinates (Goring and Nikora 1998; García *et al.* 2005). The power spectra can then be reverse Fourier transformed to generate a noise filtered time series. For some applications it is also possible to remove the bias from Doppler noise in the time domain (e.g., Thomson *et al.* 2010 for turbulence intensity).

3 ORNL ADV DATA POST-PROCESSING METHODOLOGY

ADV data need to be processed in order to detect, remove and replace invalid data (outliers). The data post-processing methodology used by ORNL offers two methods to filter outliers, which are correlation filtering and Phase-Space Threshold (PST) filtering. PST filtering includes the original and the modified versions. Three schemes are provided to replace the data that are identified as outliers. These are replacement by the overall average, by the previous valid point and by polynomial interpolation. This chapter describes the algorithms of the ADV data post-processing code and provides guidance on running the program.

3.1 ALGORITHM

The algorithm of the ORNL ADV data post-processing code is written in MATLAB and consists of several independent functions that are called by the main program (Figure 3.1). The first step is to export the ADV data into the MATLAB workspace. If the data are in the Microsoft Excel - compatible format, such as *.csv, the MATLAB function *xlsread* would be convenient to use as it detects and removes the unused file headers easily. The user is given the choice whether to implement data filtering based on the correlation threshold or not. If correlation filtering is selected the user specifies the threshold value. The outliers can be replaced by selecting from three replacement methods, or the user can choose not to replace the data. The number of outliers is then computed and the user will be given the option to draw the velocity time series (3 velocity components) with the outliers marked with red circles.

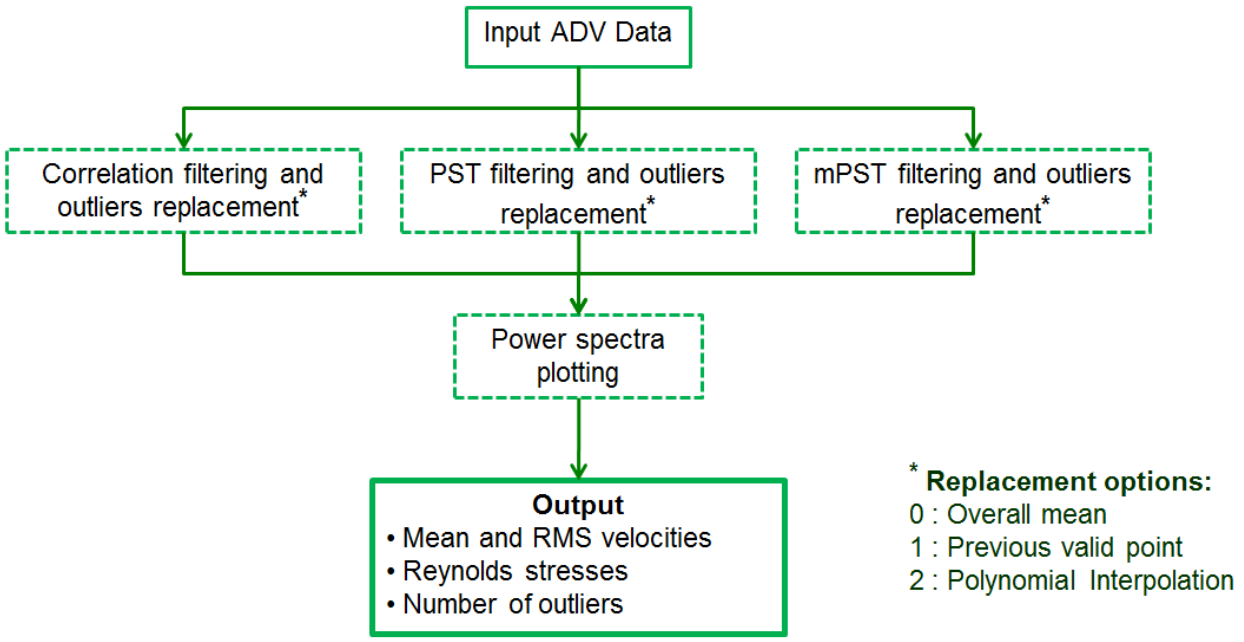

Figure 3.1 Algorithm adopted for the ORNL ADV data post-processing methodology – the steps in dashed line boxes are optional.

The user is then given choices whether to implement Phase-Space Threshold (PST) filtering, modified Phase-Space Threshold (mPST) filtering or to bypass PST altogether. When the PST or mPST filter is chosen, the number of outliers is computed and the user will be given the option to plot the velocity time series and the ellipsoid that delineates the threshold for outliers. Once the filtering process is completed, the user is given the option to plot the velocity power spectra. The user inputs the sampling rate of the ADV used during measurements if this option is chosen.

3.1.1 Phase-Space Threshold method

The Goring and Nikora (2002) PST algorithm employs a three-dimensional Poincaré map (phase-space plot) in which the fluctuating component of a time series and its first and second time derivatives are plotted against each other. Calculation of the standard deviations of the variables in each dimension and the rotation angle of the principal axis are used to construct an ellipsoid, which denotes the boundary of the Universal criterion. Any points lying outside of this ellipsoid are designated as spikes and are removed and replaced.

Goring and Nikora (2002) do not specify an optimal method of replacement, though they mention the following as their replacement options: overall average, previous value, linear interpolation, and cubic interpolation using twelve points on either side of the removed point (their recommended method).

The replacement method is iterated until no points lie outside of the ellipsoid or the maximum number of iterations is reached. The ellipsoid may shrink upon iteration corresponding to the diminishing standard deviations of the velocity during subsequent iterations. No effect on further replacement is defined as a condition in which the spikes that are identified in one iteration are the same as those identified in the previous iteration; and therefore, would be identified in any subsequent iteration without change.

Parsheh *et al.* (2010) adapted the algorithm described by Goring and Nikora (2002), but shared the widely held concern that the method in previous implementations identified several data points as spikes that were valid according to Parsheh *et al.* (2010). They also considered the effects that filtering has upon the power spectra and prescribed their so-called modified Phase-Space Thresholding Sample and Hold algorithm (mPST-SH).

The mPST-SH algorithm evaluates the validity of data in three stages. First any velocity measurements near the average are incontrovertibly marked as valid. Then any data found to be notably far from the average are marked as invalid and are removed. The user provides input variables to determine the meaning of near and far. Finally the data are subjected to modified phase-space thresholding in which the median of the absolute deviation is used rather than the standard deviation since the former is more robust and values termed as spikes are replaced. However, if any of the data points that the PST filter identified as spikes were previously identified as incontrovertibly valid (those near the average), they are not replaced. Parsheh *et al.* (2010) adopted replacement by the last valid point as their replacement strategy and did not examine the effects of other replacement methods.

3.1.2 Data replacements

The replacement function allows the user to select from among replacement data by the overall average, by the previous valid point, or by polynomial interpolation. As emphasized earlier, replacement is not aimed to reconstruct the dataset, which would have been measured when errors in the dataset do not exist; but rather, to fill in the data gaps so that they are continuous with respect to time, which is the prerequisite for power spectra computation. It is always a good practice to compare the results from the different replacement methods.

3.1.3 Spectral energy density

One of the characteristics of turbulence is the apparent randomness of velocity fluctuations with respect to time. The statistical properties of turbulence, however, are not random. The instantaneous value of a velocity component (u) can be decomposed into the time averaged velocity (U), which has a constant value for uniform flow, and the fluctuating component (u'), which has an apparent random value with respect to time (Figure 3.2). The spectral energy density (SED) is calculated by decomposing the time series of instantaneous velocity into a set of periodical sine and cosine functions with various amplitudes and frequencies, then plotting the amplitude of each periodical function versus their frequency on a log scale. The frequency of the periodical functions is inversely proportional to the time scale of the eddies, and hence, their size. Large eddies correspond to the lower frequency domain and vice versa. Nezu and Nakagawa (1993) suggest that the minimum sampling frequency of the instrument should be greater than $\frac{50U}{\pi H}$ to analyze the spectral distribution down to the viscous subrange.

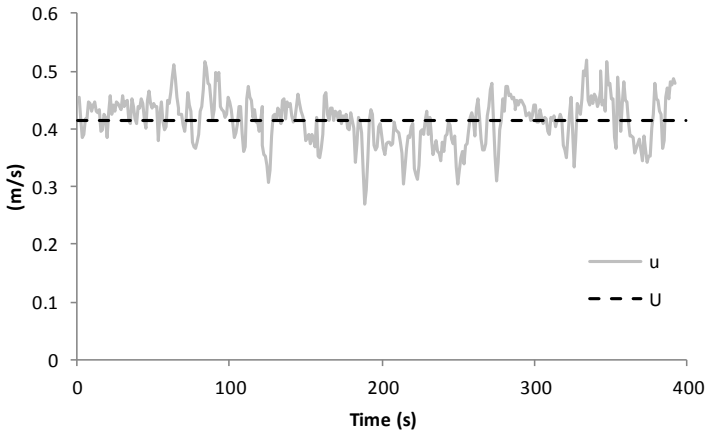

Figure 3.2 Decomposition of u into U and u'.

The SED can be computed via the autocorrelation of velocity where the autocorrelation of the streamwise velocity component is expressed as

$$R_{uu}(\tau) = < u(t)u(t+\tau) > \tag{3.1}$$

and u = velocity component in the streamwise direction, t = fixed time, τ = time shift and < > denotes ensemble averaging (Landahl and Mollo-Christensen 1992). The SED of Equation (3.1) for a discrete measurement time of T can be expressed as

$$S_{uu}(T,f) = \int_{-T}^{T} R_{uu}(T,\tau) e^{-i2\pi f\tau}\, d\tau = \frac{|S_u(T,f)|^2}{T} \tag{3.2}$$

where S_u is the Fourier transform of u, f = frequency band, i = imaginary unit number with $i^2 = -1$ (Pope 2000; Howard 2002). The ORNL ADV data post-processing code computes the SED using the expression on the right hand side of Equation (3.2). The proof of the equality expressed by Eqn. 3 can be found in Howard (2002, page 81). It first computes the SED of the fluctuating component of the velocity, squares its absolute value and then divides it with the total sampling time. The spectral energy densities contained beyond $½f_R$ experience aliasing, which constitutes a potential source of error (Bendat and Piersol 1971, page 28). Hence, only the spectral energy densities contained up to $½f_R$ (often termed as the Nyquist or folding frequency) are plotted. Presently the maximum sampling rate of a commercially available ADV is 200Hz. Therefore 100Hz is the maximum spectral energy plotted in the SED (e.g., Figure 3.3) if this maximum sampling rate is used.

Spectral leakage occurs due to the existence of SED values within a frequency band not represented in the fast Fourier transform (*fft*) computation. The power in that frequency band leaks to the neighboring bands, often resulting in a fluctuating SED curve (see Bendat and Piersoll 1971 for more details). A window function is often used to attenuate the fluctuations. The ORNL ADV data post-processing code uses 50% overlapping windows by default, where the user provides the number of windows (*nwin*) to be used as input. An *nwin* value of 1 will not apply this smoothing technique. Higher values of *nwin* increase smoothing (Figure 3.3), but increases the minimum frequency of the SED. An *nwin* value will have a different smoothing level in two datasets if the number of samples of those datasets is different. In order to have a similar level of smoothing, a dataset with a high number of samples requires a higher *nwin* value than the *nwin* value used for a dataset with a low number of samples. When the SED plot is used to determine the peaking of energy at a certain frequency, and its peak value, the user should recognize that the magnitude of the peaks may change with the smoothing level.

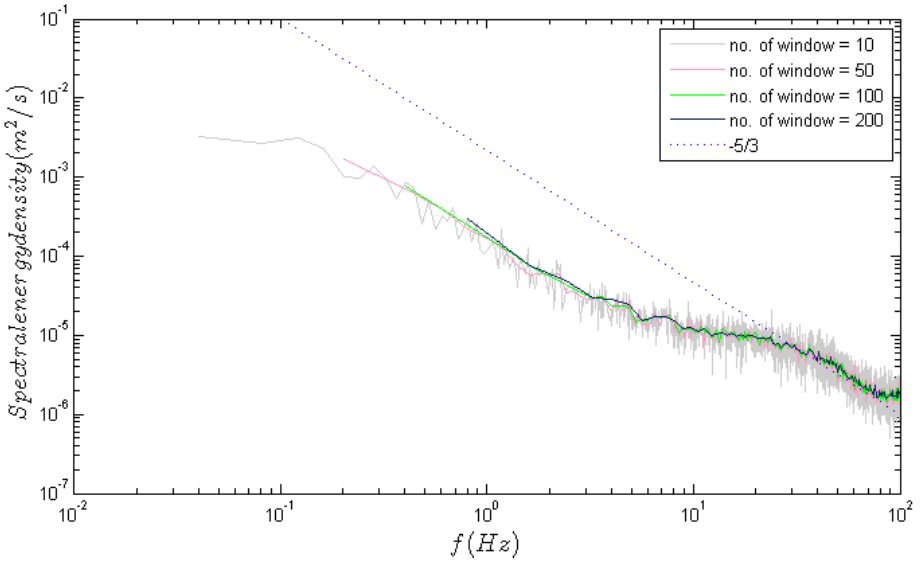

Figure 3.3 Spectral energy density plot for *u* at z = 0.425m.

3.2 INPUT/OUTPUT

At the time this report is being written, the ORNL ADCP data post-processing code is being compiled in order to provide users with a standalone program that can be run without having the MATLAB software. An example ADV post-processing analysis using the ORNL code advfilter.m is presented in this section. The code requires the ADV's three components of velocity and correlation scores as input. The *X*, *Y* and *Z* components of the velocity must be in columns 3, 4 and 5 of the MATLAB array and the correlation scores must be in columns 9, 10 and 11. This configuration is standard for files converted with Sontek Horizon ADV software. The code is capable of processing multiple input files at once. One of the most convenient ways to input the data into MATLAB is by converting the ADV data into a comma separated value (*.csv) file that can be imported to MATLAB. The details of each output variable are listed in Table 3.1. In addition, the code can also plot the Poincaré map and velocity time series for PST and mPST methods, and the SED plots. When processing multiple datasets only the last dataset is plotted.

Table 3.1 Output file generated by ORNL ADV data post-processing code

No.	Output file name	Description
1	M.txt	A matrix with columns [*U*, U_{RMS}, *V*, V_{RMS}, *W*, W_{RMS}]. RMS is one of the fluctuating components, the means are the arithmetic means of velocities *u*, *v*, and *w* (the *X*, *Y*, and *Z* components).
2	Reynolds.txt	A matrix of the Reynolds stresses [$\overline{u'u'}$, $\overline{u'v'}$, $\overline{u'w'}$, $\overline{v'v'}$, $\overline{v'w'}$, $\overline{w'w'}$].
3	Correlation_Filter.txt	A matrix of the number of outliers detected using the correlation filter [no. of outliers, no. of outliers in percentage].
4	PST_Filter.txt	A matrix of the number of outliers detected using the PST (or mPST) filter [no. of outliers in percentage for *A/X/U* component, no. of outliers in percentage for *B/Y/V* component, no. of outliers in percentage for *C/Z/W* component].
5	Ptnos.txt	A matrix of the total number of samples [number of samples]
6	Spectra(i).txt	A matrix that saves the velocity spectra results [frequency, A/X/U component of the velocity spectra, *B/Y/V* component of the velocity spectra, C/Z/W component of the velocity spectra]. The number of the output files created is the same as the number of input files.

3.3 EXAMPLE POST-PROCESSING ANALYSIS

The results from different filtering and replacement schemes are compared and analyzed below to provide a demonstration of the ORNL ADV data post-processing code. Three data filtering schemes are considered: correlation filtering, PST filtering and mPST filtering (with *C1* = 1.1 and *C2* = 1.5 only). For each case three data replacement methods are considered: replacement by the overall average (option 0), replacement by the previous valid point (option 1) and replacement by polynomial interpolation (option 2). The number of outliers detected, mean velocity, RMS velocity and power spectral densities (SED) are reported for each case. The measured data used for this analysis were obtained in the SAFL main channel flume shown in Figure 3.4 below. Generally instantaneous velocity measurements contain less erroneous values in a controlled laboratory environment compared to the field.

3.3.1 Description of the data

The ADV data used for the analysis consists of 41 point measurements at 25mm intervals in a vertical profile. The measurements were obtained at the centerline of the 2.75m wide SAFL flume 1m upstream of a 1:10 scale model of an MHK turbine with a 0.5m blade diameter. Instantaneous velocity measurements were taken at a 200Hz sampling rate using a Nortek Vectrino ADV with four receiving transducers, fixed to a computerized traversing system (cart) capable of moving the ADV within 1mm accuracy, shown in Figure 3.4. The horizontal velocity range of the ADV was set at 0.84m/s. The water depth (*H*) during the measurement was kept constant at 1.15m. The hub of the turbine model was located 0.425m above the mean bed elevation of the flume.

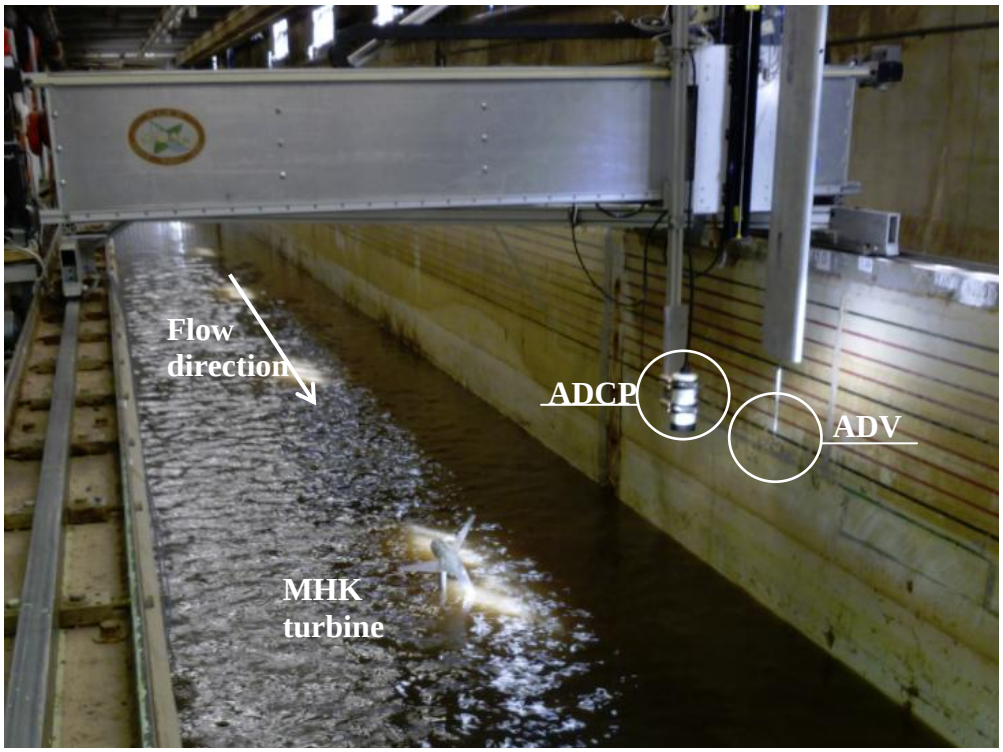

Figure 3.4 Flume at the St. Anthony Falls laboratory (University of Minnesota) where the ADV data were obtained, facing upstream.

3.3.2 Percentage of outliers

Varying the correlation cutoff percentage from 50% to 70% yields a significant difference among the number of outliers detected (Figure 3.5). The higher percentage of filtered data is observed for the points located near the bed. Cutoff values of 50%, 60% and 70% correspond to ~2%, ~4% and ~10% filtered data. The velocity measurements become less well correlated near the bed due to increased turbulence levels near boundaries (Martin *et al* 2002). At high levels of turbulence particles in the water will not maintain their relative positions with respect to each other, which increases the Doppler noise level of the return signal. As reported by Martin *et al.* 2002, increasing the velocity range will increase the correlation values. However, such an approach will decrease the measurement accuracy and should be applied with caution.

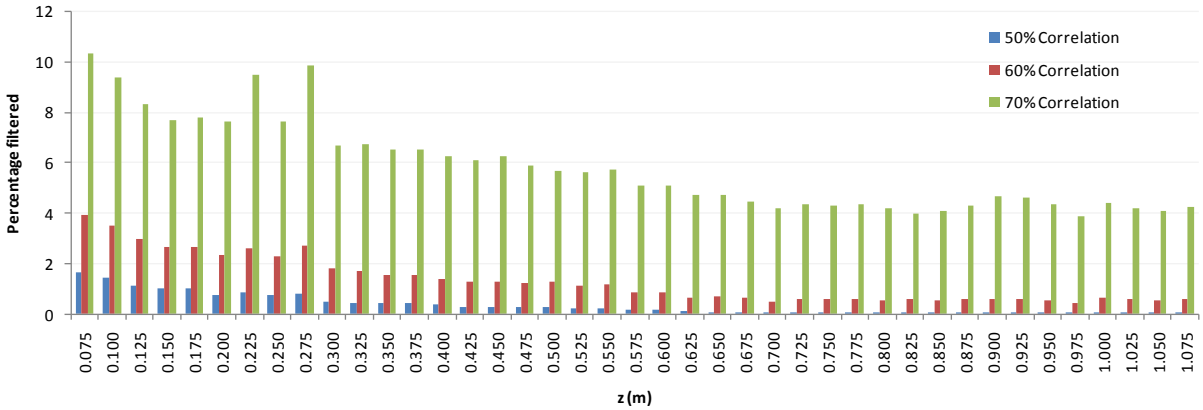

Figure 3.5 Number of outliers (in percent) for different correlation filter value.

The PST and mPST filters also detect a higher number of outliers in the near bed region (Figure 3.6). The number of outliers detected for measurements at $z > 0.700$m is less than 1% of the total number of data and are not shown in Figure 3.6. Note that the number of outliers is different for each replacement scheme because the outliers are replaced at each iteration in the PST and mPST methods. The number of outliers does not exceed 5% of the total number of data for the *X* and *Y* velocity components (*u* and *v*). In contrast, the *Z* velocity component (*w*) has a high number of outliers, up to ~15%, compared to those for *u* and *v*.

At a certain location near the bed the reflection of a previous pulse by the boundary can return to the receive transducer at the same time as the current pulse, causing interference. The relatively high number of outliers observed at $z = 0.125$m for the *X* and *Z* components is likely a result of this boundary/bed interference, a condition commonly referred to as a 'velocity hole' or 'weak spot' (Lane *et al*. 1998 and Craig *et al*. 2010). The standard deviations of *u* and *w* at $z = 0.125$m are twice of those for the *u* and *w* at the neighboring locations ($z = 0.100$ and 0.150m). Figure 3.7 compares all three components of the instantaneous velocity time series at this velocity hole with those at z = 0.425m (hub height). The comparison illustrates the noise resulting from this interference effect. The location of this velocity hole depends on the type of the ADV and the velocity range setting. An adjustment of the velocity range setting is recommended to correct for this interference. This example illustrates the benefits of PST and mPST filtering for detecting velocity holes relative to correlation filtering. A high correlation value simply indicates that the system measured the two pulses it originally sent out and is determining a valid phase shift. However, high correlated data contain spikes that can only be detected with PST or mPST filtering.

One of the goals of noise filtering is to reduce the variance of the velocity data caused by noise, but retaining the variance caused by the turbulent velocity fluctuation. Table 3.2 shows that PST filtering followed by replacement with the overall average reduces the variance of *u* of the highly fluctuated data ($z = 0.125$m) to approximately the same value where velocity holes do not occur (e.g., $z = 0.425$m). The 70% correlation filter, however, fails to reduce the variance of *u* to a similar level. Low correlated data that have similar statistical properties (e.g., magnitude of velocity fluctuation, mean velocity) to the high correlated data are often valid data that should not be discarded.

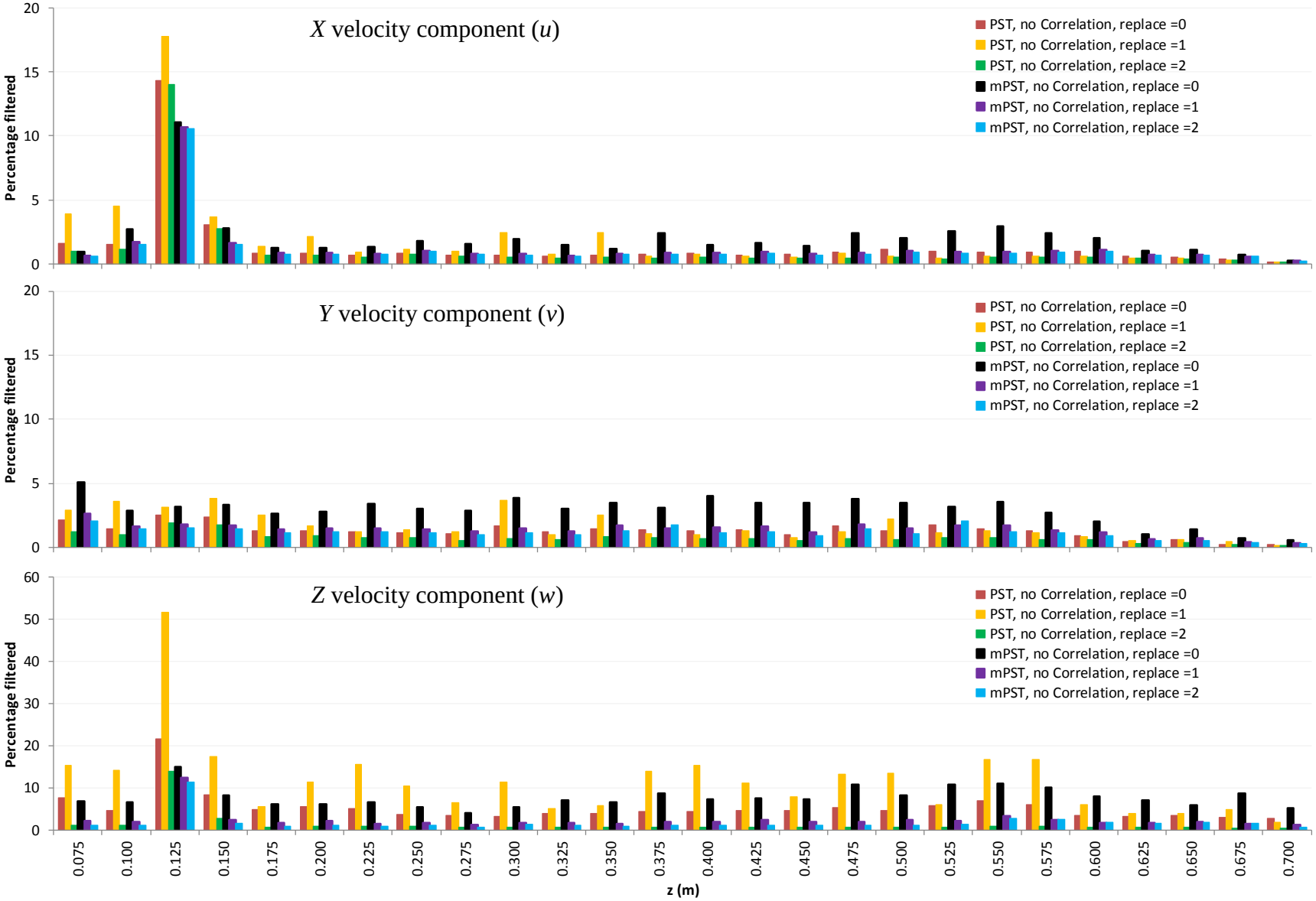

Figure 3.6 Number of outliers (in percent) for PST and mPST filters with different replacement options.

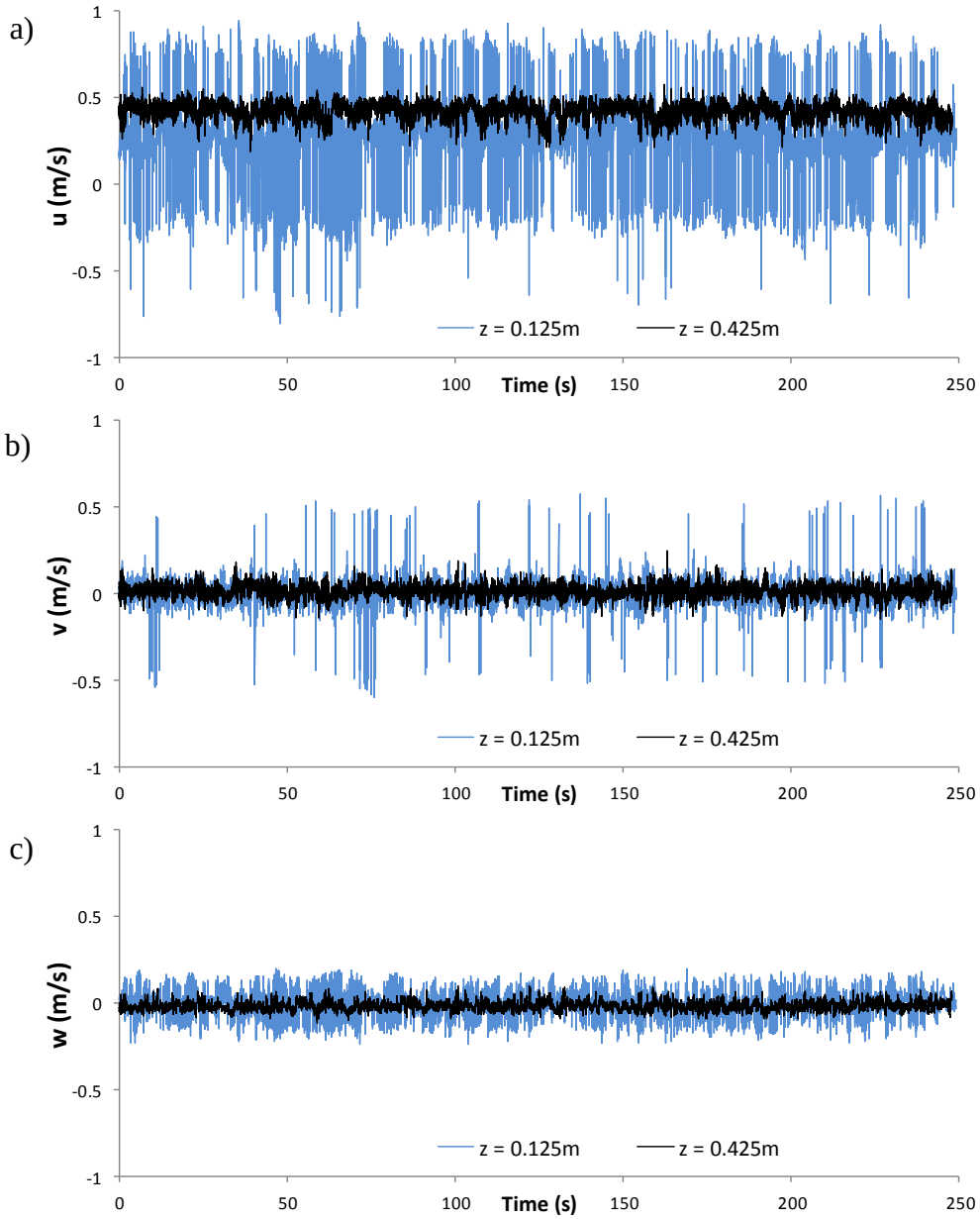

Figure 3.7 Velocity timeseries at z = 0.125m and 0.425m.

Table 3.2 Variance of *u* for the raw and post-processed data.

	z = 0.425m	*z* = 0.125m
Raw data	0.0018	0.0286
PST with replacement by the overall average	0.0017	**0.0033**
Correlation filter (70%) with replacement by the overall average	0.0017	0.0258

3.3.3 Mean velocity and velocity RMS (standard deviation)

Figure 3.9 shows the mean velocity of the *X*, *Y* and *Z* components (*U*, *V* and *W*) for the raw data and the 70% cutoff correlation filtered data. Varying the cutoff values (50%, 60% and 70%) for the correlation filter only has a minor effect on the mean velocity profiles in all components, which is an indication that the outliers are equally distributed on both sides of the mean in the velocity histogram. This condition can clearly be seen for the data at z = 0.125m in Figure 3.9. The filtered data for other cutoff and replacement values are not shown because they are similar to both the raw and the 70% cutoff correlation filtered data. The values of *U* do not change from the raw data by more than 1.5% for all of the cases being investigated. The values of *V* and *W* do not typically change more than 3% from the raw data, except for the near bed region where the difference can reach up to 10%. Note that *U* at the closest point to the bed (z = 0.075m) deviate from the general trend of the velocity distribution. The data at this location contain error caused by the movement of the ADV at the end of the measurement and should be discarded. However, they are shown here for illustration purpose.

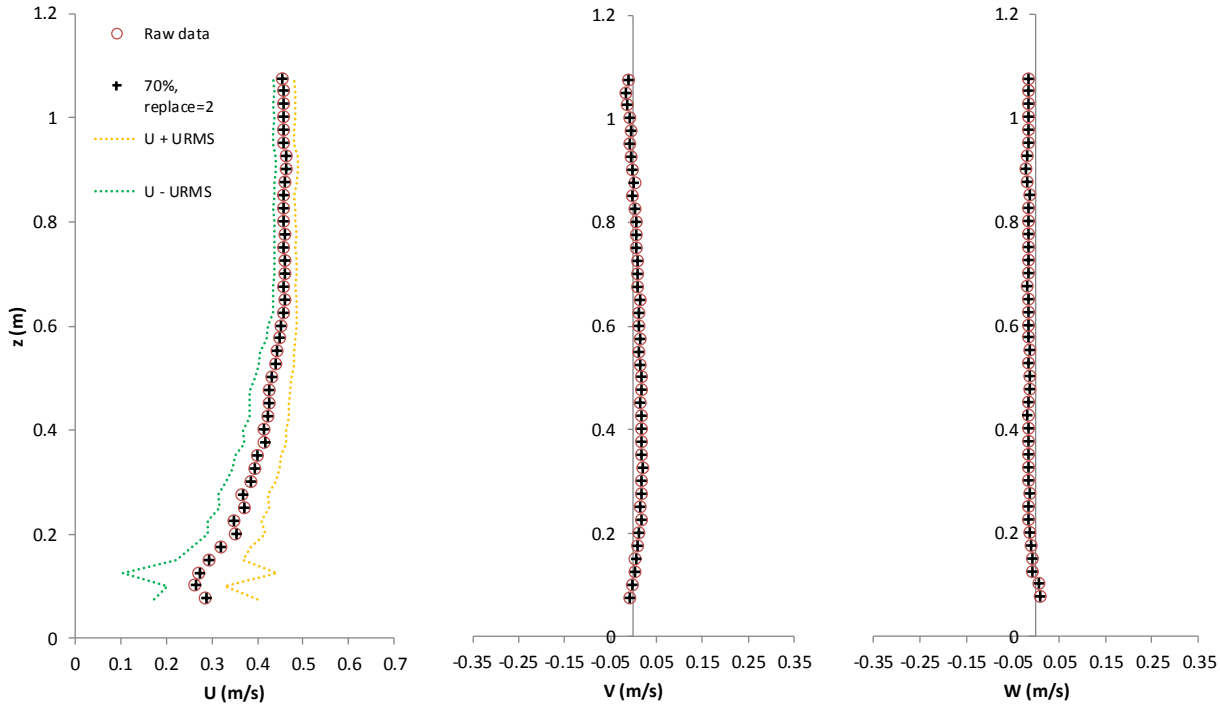

Figure 3.8 Mean streamwise, lateral and vertical velocities with respect to distance from bed for the raw data (0%) and the 70% cutoff correlation filtered data.

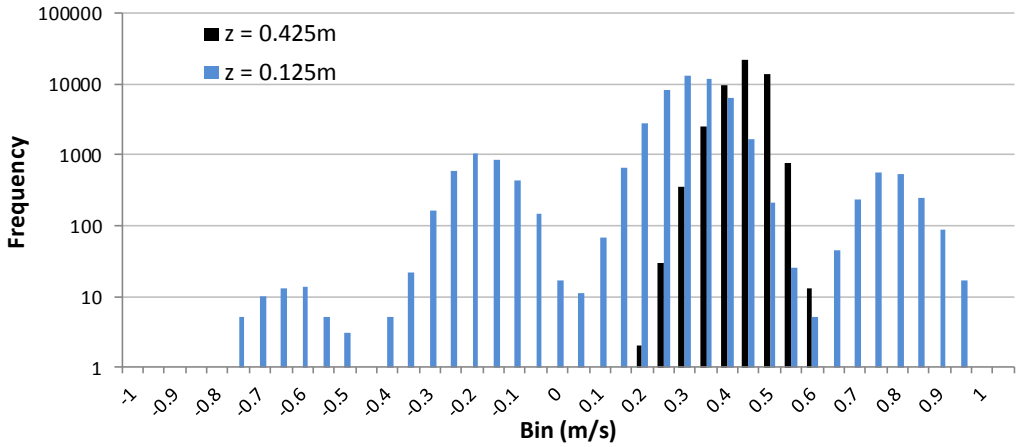

Figure 3.9 Histogram of u for z = 0.425 and 0.125m.

Data filtering using a 70% correlation cutoff does not change the RMS values of velocity significantly for most of the data, as shown in Figure 3.10. Only for the 70% cutoff with replacement scheme 0 (overall average) do the U_{RMS} values differ by up to 8% from the raw data (see Appendix 1 for graphs showing the differences of mean velocity and mean velocity RMS between the raw data and filtered data). Replacement using polynomial interpolation (replace = 2) should be used with extra care because it may replace outliers with an extremely high or low data value if many outliers are clustered together in one segment. An example of this condition is shown in Figure 3.11. The mean velocity RMS for the replacement 2 at several points are higher than that for the raw data for the same reason (Figure 3.10).

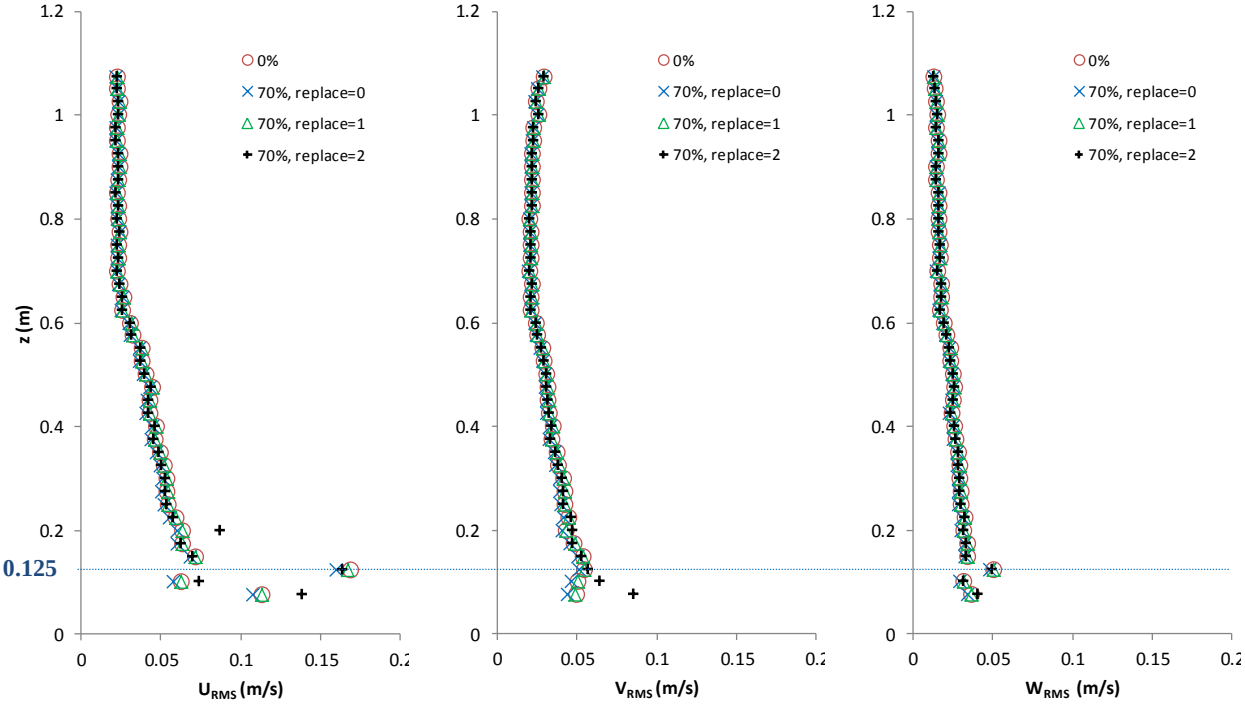

Figure 3.10 RMS values of streamwise, lateral and vertical velocities with respect to distance from bed for the raw data (0%) and the 70% cutoff correlation filtered data.

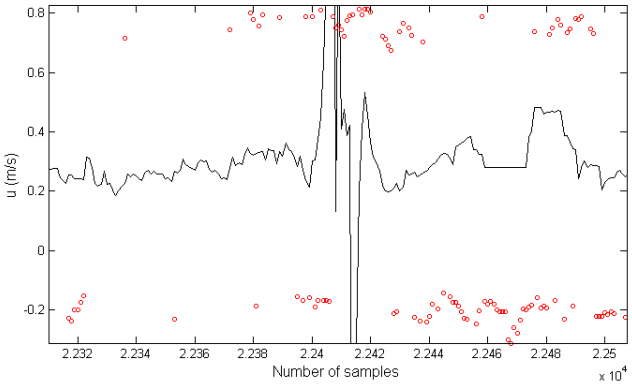

Figure 3.11 Outliers replacement for 70% correlation cutoff with polynomial interpolation – red circles are the outliers being replaced, black lines are the velocity time series after outliers are being replaced.

Similar to the correlation filtered data, the U, V and W of the PST and mPST filtered data do not depart significantly from the raw data. The mPST with an overall average replacement (replace = 0) gives slightly reduced values than the raw data for U_{RMS}, V_{RMS} and W_{RMS}, while the PST with overall average tends to give higher values in several occasions (Figure 3.12). The W_{RMS} calculated from the data filtered and replaced using mPST filtering with polynomial interpolation replacement has much higher values at two points due to clustering of the outliers, which yields an error in the replacement calculation. PST and mPST methods clearly provide an improvement at z = 0.125m, by reducing the mean RMS velocities to the values that follow the trend of the overall dataset.

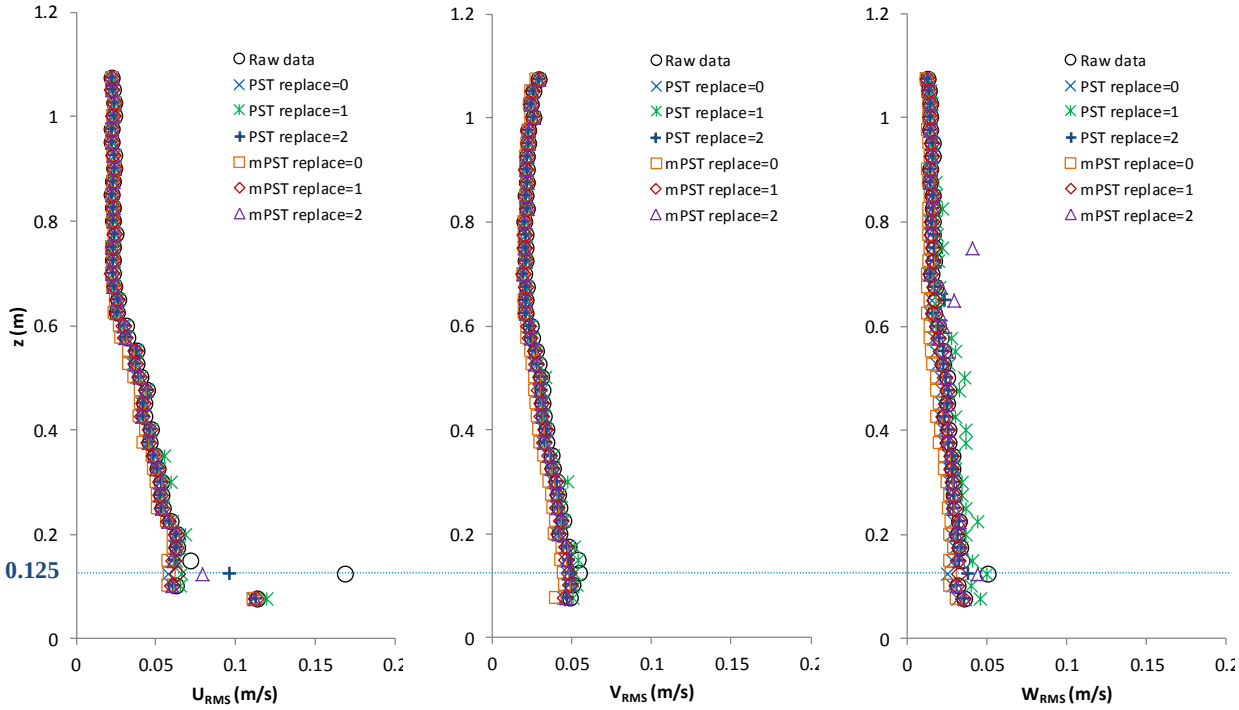

Figure 3.12 RMS values of streamwise, lateral and vertical velocities with respect to distance from bed for PST and mPST filtered data.

3.3.4 Spectral energy density

The correlation filter method provides no improvement to the SED plots when the raw data contains a significant number of spikes that increase spectral energy densities, e.g., at z = 0.125m, (Figure 3.13). In contrast the PST and mPST methods are recommended because they significantly improve the accuracy of the spectral energy density (Figure 3.13) when numerous spikes are present. Care should be taken, however, when using the polynomial interpolation replacement (replace = 2) as the resulting SED plots can show strange behavior (Figure 3.14a, d and f); although these anomalies may be improved if the user changes the interpolation parameter to a different value. Replacements by the overall average and previous valid point appear to give more reasonable results and are therefore recommended; although there is a tendency for the replacement by the previous valid point to overestimate the SED approximation of the replacement by the overall average at low frequencies, while underestimating at higher frequencies.

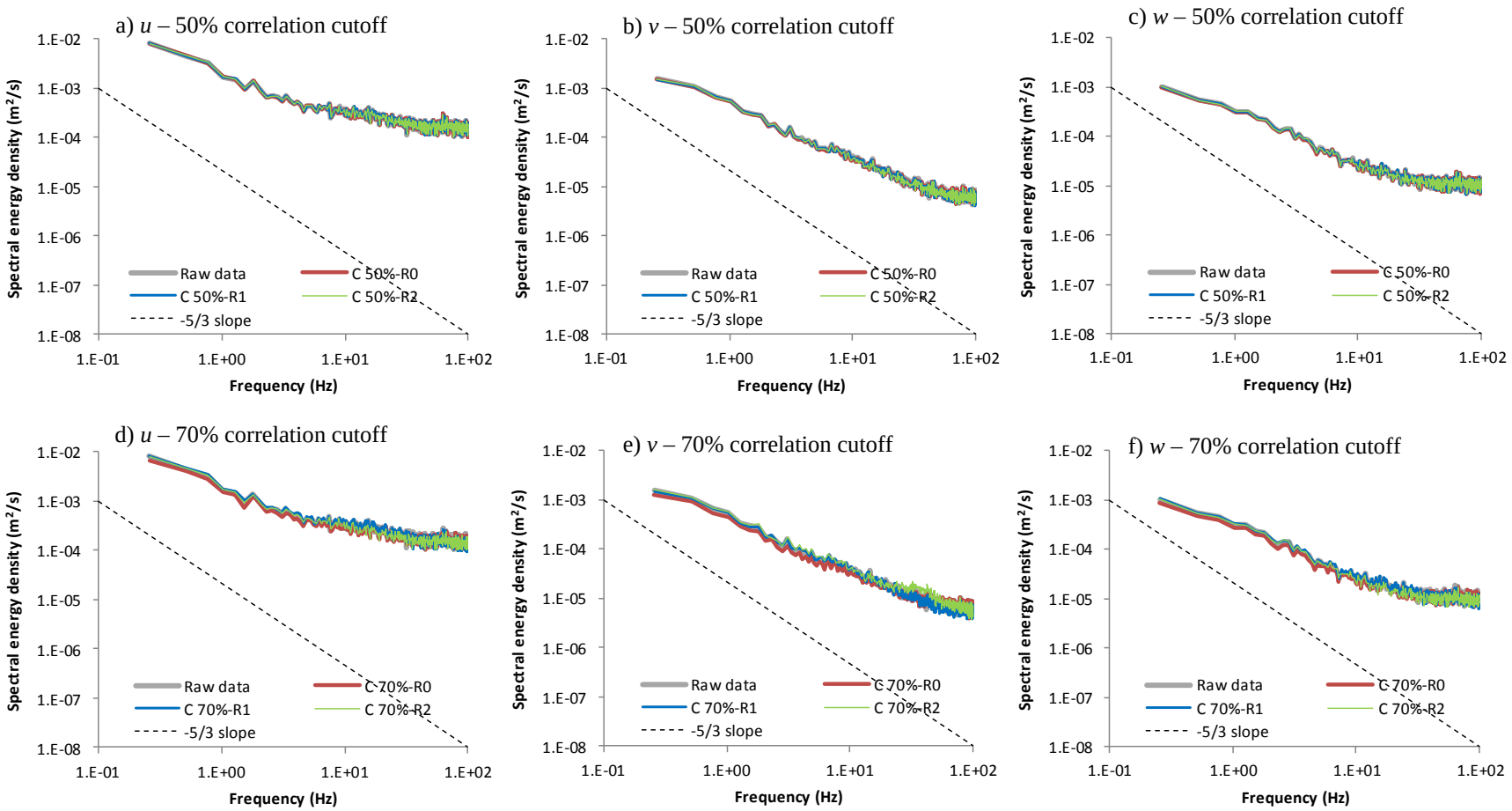

Figure 3.13 One dimensional spectral energy density for correlation filtered data at z = 0.125m.

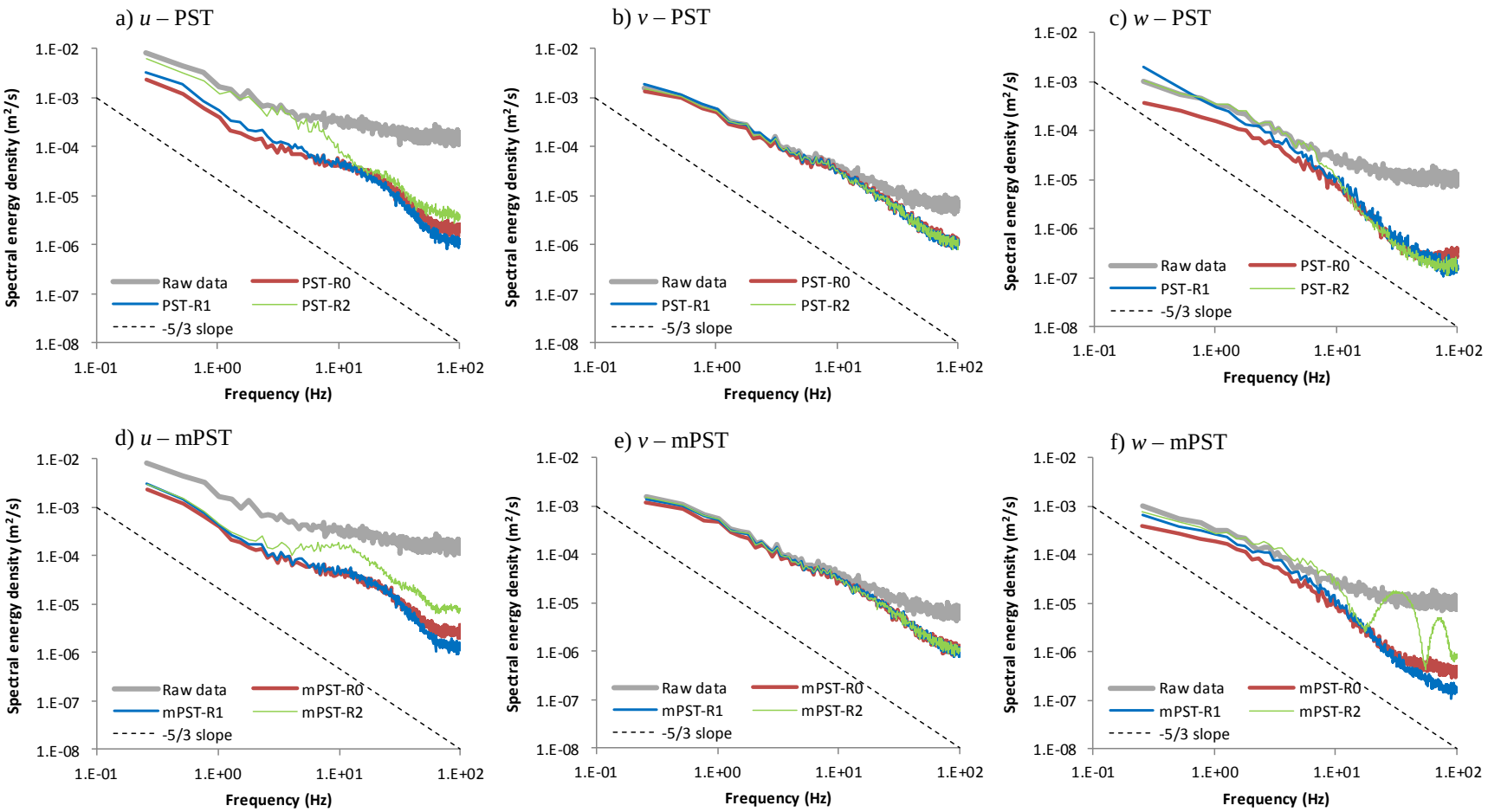

Figure 3.14 One dimensional spectral energy density for PST and mPST filtered data at z = 0.125m.

3.3.5 Summary

The subsequent analysis of SAFL flume instantaneous velocity time series outlined in sections 3.3.2 – 3.3.4 leads to the following conclusions:

- There is no significant improvement in the mean velocities from the raw data, when the data are processed using a correlation or PST filter because the outliers are equally distributed on both sides of the mean in the velocity histogram (Figure 3.9).
- PST and mPST filtering methods successfully filter data contaminated with spikes (e.g., $z = 0.125$). Both methods reduce the RMS/standard deviation of the velocity data contaminated with spikes (Figure 3.12, Table 3.2) and should be used before calculating turbulence intensities and Reynolds stresses. No less important, PST and mPST filtering does not alter the mean velocity and velocity RMS of valid data (Figure 3.10).
- Data with high correlations only indicate that the system measured the two pulses it originally sent out and that the phase shift is valid. However, data with high correlations may contain spikes.
- Correlation filtering with 50, 60 and 70% cutoff values does not significantly reduce the RMS/standard deviation of the velocity data associated with the spikes because low correlated data may be valid, i.e., they are not spikes and may have similar statistical properties to the high correlated data.
- Replacement using polynomial interpolation (replace = 2) may replace outliers with an extremely high or low replacement value if many outliers are clustered together in one segment, which will significantly affect the velocity RMS and spectral energy density (Figures 3.14a, d, f). Replacements by the overall average and the previous valid point appear to give more stable results in the spectral energy density plot.
- PST and mPST methods provide an improvement by significantly reducing the spectral energy densities of raw data contaminated with a significant number of spikes (Figure 3.14). The correlation filter method, on the other hand, offers no similar improvement (Figure 3.13)
- The PST does not require parameterization, which is considered a practical advantage over the mPST method.

4 PRE- AND POST-PROCESSING STEPS

The following steps are recommended when post-processing instantaneous velocity time series ADV measurements. While the data post-processing methodology can reduce errors, preventive measures to minimize errors during measurement should be undertaken whenever possible. Low correlation values and errors due to signal aliasing and boundary interference can be avoided by setting the velocity range correctly before undertaking measurements. The first step is to make sure there are no empty values within the instantaneous velocity time series data, which will prevent the code from running. Extreme velocity values beyond the instrument capability, typically up to 7m/s for ADVs, may bias the post processing results. It is recommended to replace such values with 'NaN' (not a number) for excluding the data and not introducing errors in the post-processing analysis. Extreme values can be easily detected in Microsoft Excel using 'min' and 'max' functions, or in the velocity time series plot, which can be called during correlation, PST or mPST filtering.

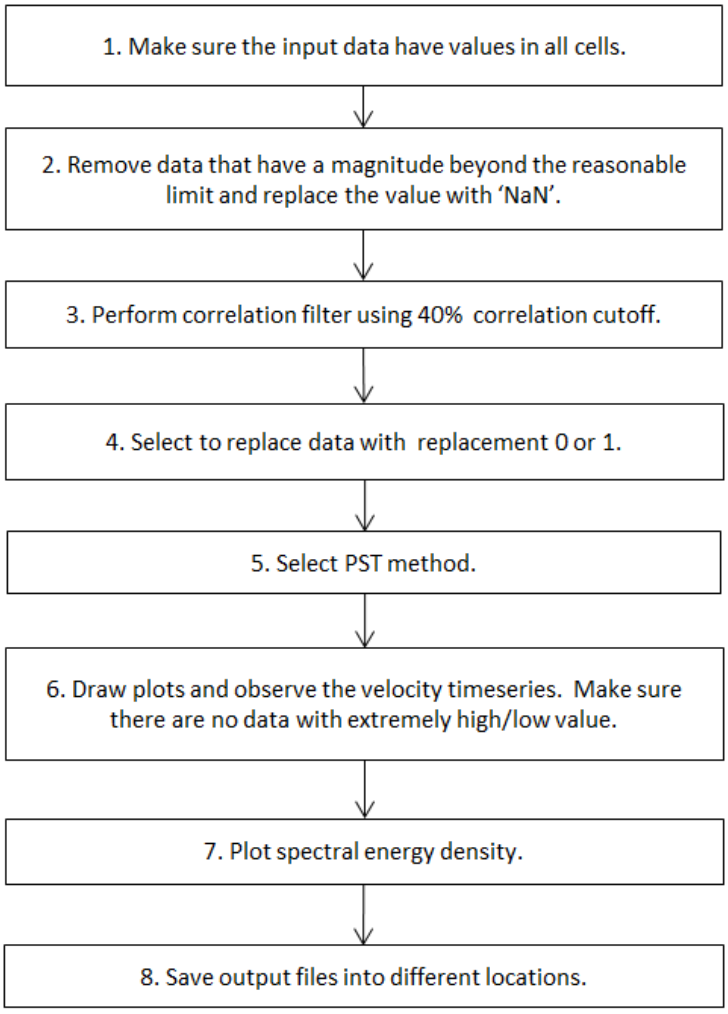

Figure 4.1 One dimensional spectral energy density for correlation filtered data at z = 0.125m.

The strategy adopted to detect outliers is to apply a low correlation filter so as not to remove legitimate data. Following the suggestion of Martin *et al*. (2002), we recommend applying a correlation filter cutoff value of 40%; and in extreme cases not applying a correlation filter if correlations are consistently below 40%. Subsequently, replacement using an overall average or previous valid point is recommended given the problems identified with the polynomial interpolation method. The PST method is recommended for removing spikes in the data. The mPST method can also be used at this step, but it requires the calibration of parameters *C1* and *C2*. After data filtering and replacement, the instantaneous velocity time series plot should be inspected to see if spikes still exist in the data. The spectral energy density should then be plotted. Finally, save all output files into different locations. Running the code again will create a new output folder that overwrites the previous output folder.

5 FUTURE WORK

The ORNL ADV data post-processing code provides an integrated tool to detect and replace outliers using different methods to improve calculations of power density and annual energy production. ADV data collected from different measurement locations can be processed simultaneously, which could save some processing time. In order to improve the capability of the code some additional functions listed below will be added in the future:

1. Calculation and plotting of velocity histograms
2. Plotting tool for mean velocity and velocity RMS
3. Calculation of two-point or space-time correlations from synchronized ADVs
4. Introduction of wavelet transforms for calculating spectra where periodic vortex shedding occurs, e.g. in the wakes of bluff bodies.

REFERENCES

Ansar, M. and Nakato, T. (2001). Experimental study of 3D pump-intake flows with and without cross flow. Journal of Hydraulic Engineering, ASCE, Vol.127(10), pp. 825-834.

Babaeyan-Koopaei, K., Ervine, D. A., Carling, P. A. and Cao, Z. (2002). Velocity and turbulence measurements for two overbank flow events in River Severn. J. Hydraul. Eng. 128, 891 (2002); doi:10.1061/(ASCE)0733-9429(2002)128:10(891).

Baldwin, J. T., Deutsch, S., Petrie, H. L. and Tarbell, J. M. (1993). Determination of principal Reynolds stresses in pulsatile flows after elliptical filtering of discrete velocity measurements. J. Biomech. Eng., v 115, I4a, pg 396-404.

Bendat, J. and Piersol, A. (1971). Random data: Analysis and measurement procedures. John Wiley and Sons, Inc.

Cea, L., Puertas, E.J. and Pena, E.L. (2007). Velocity measurements on highly turbulent free surface flow using ADV. Exp Fluids 42:333–348 DOI 10.1007/s00348-006-0237-3.

Craig, R.G.A., Loadman, C., Rusello, P.J., Siegel, E. and Clement, B. (2010). Characterization and testing of a new bistatic profiling acoustic Doppler velocimeter: The Vectrino-II. Proceedings of the IEEE/OES/CWTM Tenth Working Conference on Current Measurement Technology.

Doroudian, B., Hurther, D. and Lemmin, U. (2007). Discussion of Turbulence measurements with acoustic Doppler velocimeters by Carlos M. García, Mariano I. Cantero, Yarko Niño, and Marcelo H. García, Journal of Hydraulic Engineering, ASCE, Vol.133, 1286.

Finelli, C.M., Hart, D.D. and Fonseca, D. M. (1999). Evaluating the Spatial Resolution of an Acoustic Doppler Velocimeter and the consequences for measuring near –bed flows. limnology and oceanography, Vol 44, #7, pp. 1793-1801.

Fontaine, A.A., Ellis, J.T., Healy, T.M., Hopmeyer, J. and Yoganathan, A.P. (1996). Identification of peak stresses in cardiac prostheses: A comparison of two-dimensional versus three-dimensional principal stress analyses. American Society Artificial Internal Organs Journal, Vol. 42, pp. 154-163.

Fontaine, A. and Neary, V.S. (2010). Experiments for Evaluating Errors in ADV Measurements due to Vortex Induced Vibrations (VIV). 2010. ORNL Technical Memorandum ORNL-TM-0802010.

Fox, J.F. and Belcher, B.J. (2009). Comparison of LSPIV, ADV, and PIV data that is decomposed to measure structure of turbulence over a gravel-bed.33rd IAHR Congress, Vancouver, BC, Canada.

García, C.M., Cantero, M.I., Niño, Y., and García, M.H.(2005). Turbulence measurements with acoustic Doppler velocimeters. Journal of Hydraulic Engineering, Vol. 131, No. 12, December 2005, pp. 1062-1073, (doi 10.1061/(ASCE)0733-9429(2005)131:12(1062)).

Goring, D. G. and Nikora, V. I. (2002). Despiking acoustic Doppler velocimeter data. J. Hydraulic Eng., 128(1) 117-126.

Goring, D. G. and Nikora, V. I. (2003). Closure to Depiking acoustic Doppler velocimeter data by Derek G. Goring and Vladimir I. Nikora. Journal of Hydraulic Engineering, ASCE, Vol. 129(6), 487 - 488.

Gunawan, B., Sun, X., Sterling, M., Knight, D. W., Shiono, K., Chandler, J., Rameshwaran, P., Wright, N. G., Sellin, R. H. J., Tang, X. and Fujita, I. (2008). An integrated and novel approach to estimating the conveyance capacity of the River Blackwater. Proceedings of the Eight International Conference on Hydro-Science and Engineering, Nagoya, Japan, September 8–12.

Gunawan, B., Sterling, M. and Knight, D. W. (2010). Using an acoustic Doppler current profiler in a small river. Water and Environment Journal, 24: 147–158. doi: 10.1111/j.1747-6593.2009.00170.x.

Hamming, R. (1983). Digital filters, 2nd Ed., Prentice Hall, Englewood Cliffs, New Jersey.

Howard, R. M. (2002). Principles of random signal analysis and low noise design: The power spectral density and its applications. Wiley-IEEE Press; 1st edition (August 8).

Holmes, R. R. and Garcia, M. H. (2008). Flow over bedforms in a large sand-bed river: A field investigation. Journal of Hydraulic Research, 46(3): p. 322-333.

Hurther, D. and Lemmin, U. (2001). A correction method for turbulence measurements with a 3D acoustic Doppler velocity profiler. J. Atmosph & Oceanic Tech., vol 18, pp. 446-458, 2001.

Hydroic, Inc. (2011). Remus 600 AUV brochure. In Kongsberg Maritime. Retrieved 9/19/2011, from http://www.km.kongsberg.com/.

Landahl, M. T. and Mollo-Christensen, E. (1992). Turbulence and random processes in fluid mechanics. Cambridge University Press.

Lane, S. N., Biron, P. M., Bradbrook, K. F., Butler, J. B., Chandler, J. H., Crowell, M. D., McLelland, S. J., Richards, K. S. and Roy, A. G. (1998). Three-dimensional measurement of river channel flow processes using acoustic doppler velocimetry. Earth Surface Processes and Landforms, 23:1247–1267. doi:10.1002/(SICI)1096-9837(199812)23:13<1247:AID-ESP930>3.0.CO;2-D.

Lohrmann, A., Cabrera, R. and Kraus, N.C. (1994). Acoustic Doppler velocimeter (ADV) for laboratory use. Proceedings of the ASCE Fundamental and Advancements in Hydraulic Measurements and Experimentation, August 1-5, 1994, Buffalo, New York.

Lohrmann, A., Cabrera, R., Gelfenbaum, G. and Haines, J. (1995). Direct measurements of Reynolds Stress with an acoustic Doppler velocimeter. Proceedings of the IEEE Fifth Working Conference on Current Measurements, St. Petersburg, FL, February 1995.

Martin, V., Fisher, T. S. R., Millar, R. G. and Quick, M. C. (2002). ADV data analysis for turbulent flows: Low correlation problem. Proceedings of Hydraulic Measurements and Experimental Methods Conference 2002. ASCE Conf. Proc. doi:10.1061/40655(2002)101.

Neary, V. S. and Sale, D. C. (2010). Flow characteristics of river resources for hydrokinetic energy conversion. Conference Proceedings, HydroVision International, July 27-30, 2010, Charlotte, NC.

Neary, V. S., Chamorro, L., Hill, C., Gunawan, B., Sotiropolous, F. and Kang, S. K. (2011). Experimental study of the effects of turbulence and large coherent structures on hydrokinetic turbines. Poster presentation. HydroVision International, July 19-22, 2011, Sacramento, CA.

Nezu, I. and Nakagawa, H. (1993). Turbulence in open-channel flows. IAHR Monograph Series, A. A. Balkema, Rotterdam.

Nikora, V. I. and Goring, D. G. (1998). ADV Measurements of turbulence: Can we improve their interpretation? Journal of Hydraulic Engineering, ASCE, Vol.p. 630-634, 1998.

Nortek. (2009). Vectrino velocimeter user guide. Retrieved 9/19/2011, from http://www.nortekusa.com/en/support/manuals.

Nystrom, E.A., Rehmann, C.R., and Oberg, K.A. (2007). Evaluation of mean velocity and turbulence measurements with ADCPs. Journal of Hydraulic Engineering, ASCE, Vol.133/12.

Parsheh, M., Sotiropoulos, F. and Port´e-Agel, F. (2010). Estimation of Power Spectra of Acoustic-Doppler Velocimetry Data Contaminated with Intermittent Spikes. Journal of Hydraulic Engineering, ASCE, Vol.136, 368 (2010); doi:10.1061/(ASCE)HY.1943-7900.0000202.

Petrie, H. L., Samimy, M. and Addy, A. L. (1988). Laser Doppler velocity bias in separated turbulent flows. Exp. in Fluids, v 6, pg 80-88.

Rantz, S.E. and others (1982). Measurement and computation of streamflow: Volume 1. Computation of discharge. U.S. Geological Survey Water Supply Paper 2175, 284 p.

RD Instruments (1996). Acoustic Doppler current profilers - Principle of operation, A practical primer. San Diego, CA, RD Instruments.

Richmond, M., Thomson, J., Polagye, B. and Durgesh V. (2010). Inflow characterization for marine and hydrokinetic energy devices. 2010. FY2010 Annual Progress Report, PNNL Annual Progress Report to DOE EERE for FY2010.

Rusello, P.J. (2009). A practical primer for pulse coherent instruments, Nortek Technical Note No.: TN-027.

SonTek (2000). Doppler velocity log for ROV/AUV applications, SonTek Newsletter, 6(1), SonTek, San Diego, CA.

SonTek (2001). Acoustic Doppler profiler technical documentation. San Diego, CA.

SonTek (2007). Horizon ADV manual. SonTek, San Diego, CA.

SonTek (2011a). 10-MHz ADV Expanded description. In Sontek Retrieved 9/19/2011, from http://www.sontek.com/pdf/expdes/10MHz-ADV-Expanded-Description.pdf.

SonTek (2011b). ADV Ocean brochures. In SonTek Retrieved 9/19/2011, from http://www.sontek.com/pdf/brochures/advocean-web-reduce.pdf.

Thomson J., Richmond M., Polagye, B. and Durgesh, V. (2010). Quantifying turbulence for tidal power applications. OCEANS 2010, MTS/IEEE.

Underwood, G.N. (1994). Evaluation of a new laboratory acoustic Doppler velocimeter. MS Thesis, Dept. of Ocean Engineering, Naval Post Graduate School, Monterey CA, 1994.

Voulgaris, G. and Trowbridge, J.H. (1998). Evaluation of the acoustic Doppler velocimeter for turbulence measurements. J. Atmosph & Oceanic Tech., vol 15, pp. 273-289, 1998.

Wahl, T. L. (2003). Discussion of Despiking acoustic Doppler velocimeter data. J. Hydraul. Eng., 129(6), 484 - 487.

Zhang, Y., Knut, S., Bellingham, J.G. and Baggeroer, A.B. (2001). Acoustic Doppler velocimeter flow measurement from an autonomous underwater vehicle with applications to deep ocean convection. J. Atmos. Oceanic Technol., 18, 2038–2051. doi: 10.1175/1520-0426(2001)018<2038:ADVFMF>2.0.CO;2.